THE FATIGUE BEHAVIOR OF DISPERSION STRENGTHENED NICKEL

THE FATIGUE BEHAVIOR OF DISPERSION STRENGTHENED NICKEL

By

MICHAEL LASH WAYMAN, B. A. Sc.

A Thesis

Submitted to the Faculty of Graduate Studies

in Partial Fulfilment of the Requirements

for the Degree

Master of Science

McMaster University

May, 1966

MASTER OF SCIENCE (1966) McMASTER UNIVERSITY
(Metallurgy Hamilton, Ontario

TITLE: The Fatigue Behavior of Dispersion Strengthened Nickel

AUTHOR: Michael Lash Wayman, B.A. Sc. (University of British Columbia)

SUPERVISOR: Professor R. K. Ham

NUMBER OF PAGES: vi, 96

SCOPE AND CONTENTS:

Fatigue and dispersion strengthening are reviewed generally. Experiments are described in which thin film transmission electron microscropy, as well as optical and electron fractography were employed to elucidate the mechanism of fatigue failure in dispersion strengthened nickel. It was found that whereas fatigue crack initiation occurs as in conventional materials, the propagation of both fatigue and tensile cracks is abnormal. The material fails in shear wherever possible although this is prevented where triaxial tensile stresses exist. Particle-matrix detachment does not occur during either tensile or fatigue stressing.

ACKNOWLEDGEMENTS

The author is greatly indebted to his supervisor Dr. R. K. Ham for suggesting the problem and providing advice and encouragement throughout the duration of the work.

The author also wishes to thank the Faculty and graduate students of the Department of Metallurgy for stimulating discussions and Mr. H. Walker for his assistance with the electron microscopy. Special thanks are also due to my wife for her patience and for typing this thesis.

Financial support in the form of a scholarship from the National Research Council is gratefully acknowledged.

TABLE OF CONTENTS

LIST OF FIGURES

CHAPTER 1

INTRODUCTION

Fatigue can be defined as the failure of a metal or alloy when a stress less than its ultimate tensile stress is applied repeatedly. In many practical cases fatigue cycling occurs between a tensile and a compressive stress. The number of cycles the material can withstand before failure is a function of the applied stress, the structure of the material, and the environment in which the stressing takes place.

This investigation is concerned with the fully reversed fatigue stressing of a dispersion strengthened alloy, TD Nickel. This is a commercially produced nickel alloy containing two volume percent thoria in the form of submicroscopic particles randomly distributed in a nickel matrix. It has been thought that dislocation or point defects produced by fatigue can be attracted to the interfaces between the particles and the matrix. Alternatively, as a result of matrix dislocations and elastic strains produced by the deformation, stresses can be generated at these interfaces particularly if they are of the noncoherent high-energy variety. Both these effects might lead to detachment of the particles from the matrix, leaving voids at the interfaces. Such voids would be expected to affect the initiation and/or propogation of fatigue cracks.

The most useful technique for observing these voids is thin film transmission electron microscopy. TD Nickel is well suited to such a study since the oxide particles are so small that they do not interfere with the electropolishing process by which thin films are produced. If voids are formed at the particle-matrix interfaces then they will be revealed by electron microscopy.

No thin film electron microscope study of the fatigue of oxide strengthened alloys has been previously reported. In fact fatigue studies of any type on these alloys are few. This investigation has therefore been planned to determine the mechanism of fatigue failure in TD Nickel.

CHAPTER 2

DISPERSION STRENGTHENING

2.1. General

A dispersion strengthened alloy may be defined as one which is made up of fine discontinuous second-phase particles randomly distributed in a matrix of pure metal or solid solution (1). Dispersion strengthening is differentiated from precipitation hardening by two factors: a non-coherent particle-matrix interface, and lack of solubility of the dispersed phase in the matrix at high temperatures. The matrix may be any metal or alloy while the dispersion may be an oxide, a nitride, a carbide, an intermetallic compound, or a pure metal. In the most useful systems the dispersed particles are stronger than the matrix.

The early history of dispersion strengthened alloys coincides with the development of SAP, sintered aluminum powder (2-5). From aluminum, experiments have been extended into numerous other systems. Recent reviews on the subject have been written by Goetzel (1,4), Guard (6), Smith (7), Kelly (8-10), and Grant (11).

Several techniques are used to manufacture dispersion strengthened alloys (11). All of these, with the exception of the overaging of precipitation-hardened alloys, involve powder metallurgy, followed by high temperature, high strain-rate consolidation to achieve

the required density. The most common techniques are:

(i) Surface Oxidation of Ultrafine Powder.

Metals which form a thin adherent oxide film are powdered, oxidized, compacted, sintered and then extruded to produce an alloy consisting of metal matrix with a dispersion of the shattered oxide which had initially formed around the metal powder particles. This method is used in the production of SAP (5).

(ii) Mechanical Blending of Fine Powders.

In this process, a fine powdered metal or alloy is blended with a much finer powdered refractory oxide (12), followed by compaction sintering and extrusion. For high temperature stability it is necessary that the free energy of formation of the matrix oxide be less than that of the refractory oxide (11).

(iii) Atomization of Alloys.

When an alloy is atomized, the quench rate is so rapid that if an intermetallic compound exists in the alloy system it precipitates as fine dendrites in the atomized droplets. Compaction and extrusion of this powder breaks up the dendrites to form an even finer dispersion. This method has been applied to the Al-$FeAl_3$ system (13); however, high temperature stability is inferior to that of oxide-strengthened alloys.

(iv) Internal Oxidation.

A dilute solid solution may be internally oxidized provided that the solute oxide has a much higher free energy of formation than the oxide of the solvent. Thin sheet or wire may be dispersion

strengthened by this method or, alternatively, powder metallurgy techniques may be used. Common systems used are Ni or Cu containing Si or Al (14-18).

(v) Decomposition of Inorganic Salts.

Thoriated nickel may be produced either by the decomposition of thorium nitrate on nickel powder (19-21) or by the deposition of a nickel compound on a thorium salt followed by co-reduction (22,23). The resultant metal powder is densified in the usual manner.

The extrusion of sintered powder can lead to stringering of the dispersed phase in the extruded direction. Since a uniform dispersion is necessary for optimization of mechanical properties this effect is undesirable. Elimination of stringering is one of the major problems in the production of dispersion strengthened alloys by powder metallurgy.

Dispersion strengthened alloys generally contain between 0.5 percent and 15 percent dispersed phase by volume. The particles may be any diameter from 50 Angstroms to more than 1 micron while interparticle separations range upward from 0.1 micron. Most of these alloys show a considerable improvement in room temperature strength over their non-dispersion strengthened counterparts. However, it is at high temperatures that they exhibit their most useful properties. Both strength and stability are vastly improved over conventional alloys at temperatures up to within a few degrees of the melting point. The high temperature properties of these materials are responsible for the impetus behind their development. Their primary applications are as components of turbines and internal combustion engines and in nuclear reactors.

2.2. Theories of the Yield Strength.

The strengthening of dispersion strengthened alloys is due to the ability of the dispersed particles to increase the stress necessary for propagation of dislocations over long distances in the matrix. The mechanisms involved are uncertain but several have been proposed and these have been reviewed by Kelly (9,10) and others (11, 24, 25). For long range dislocation motion in these alloys it is necessary either that dislocations by-pass the particles (by bowing between them, cross-slipping around them, or cutting through them) or else that new dislocation sources are created. All theories of the yield strength assume that particles are not detached from the matrix.

Several relationships have been postulated which relate the yield strengths of these alloys to a parameter of the dispersion. The differences between these relationships are quite marked, however, the lack of agreement among the results of various investigations is equally marked. These disparities are due to structural differences in the many systems which have been studied. Such structural differences include (11) differences in particle size, shape and distribution, in matrix composition, in the particle-matrix interfacial energy, in the coherency of the particle-matrix bond, in the degree of cold work of the matrix and in the mechanical properties of the dispersed phase.

In general, strength increases and ductility decreases as particle size and/or interparticle spacing decrease. However, several different relationships have been proposed.

(i) The first such relationship was determined empirically by Gensamer (26) who found for pearlitic and spheroidized steels that the yield stress is inversely proportional to the log mean free ferrite path. Agreement with this relationship has been found in carbon steel (27), SAP (28), tempered martensite (29) and internally oxidized copper (16). However, Shaw et al (30) found for overaged aluminum-copper that the relationship

$$\text{Y.S.} \propto \frac{1}{\lambda^n} \quad \text{where} \quad \begin{array}{l} n \text{ is a strain dependent parameter} \\ \lambda \text{ is volume mean free path} \end{array}$$

gave a better fit to their experimental results. Westbrook (31) applied a similar relation devised by Unckel (32)

$$\text{Y.S.} \propto e^{-\beta\lambda} \quad \text{where } \beta \text{ is approximately .06}$$

to the results of other investigators (26,27,30) including Gensamer and Shaw. He found that Unckel's function fitted their results at least as well as did their own relationships. In addition, Unckel's function is much more accurate at large and small inter-particle spacings. However, all these relationships are empirical.

(ii) An alternative relationship has been derived fundamentally by Orowan (33) using concepts developed by Nabarro (34). This predicts that yield stress is inversely proportional to the mean planar spacing between particles, i.e. the spacing as seen by a moving dislocation. This distance is considerably less (35) than the mean free path which is derived from intercepts on random straight lines drawn across micrographs of cross-sections of the alloy. According to Orowan, yield

occurs when the applied stress is sufficient to force dislocations between particles lying in the slip plane, leaving concentric dislocation rings around each particle. For the Orowan criterion to be valid, the particle spacing must be such that little dislocation motion occurs in the matrix before the dislocations come into contact with the particles so that no work hardening of the matrix has occurred (9). Thus the Orowan relationship should not apply to dispersion-strengthened alloys manufactured by powder metallurgical processes (which involve extrusion and swaging) unless they are completely recrystallized before testing. However, many investigators (12,18,19,36-38) have found agreement with the Orowan relationship despite the fact that the matrices of several of their systems (12,19,36) were in a strain hardened condition. In addition, Tyson (39) has re-analyzed the data of other investigators (27,29) whose results agreed with the Gensamer relationship. He converted mean free paths to interparticle spacings and found that the Orowan prediction was obeyed. It is significant that in all investigations in which the conditions for Orowan's criterion were met, agreement was obtained (25). In addition, transmission electron microscopy has revealed dislocations bowing between particles (18,38,40-42) and leaving loops around them (43) as predicted.

(iii) Ansell and Lenel (44-49) have proposed a yield mechanism based on a different concept. According to these workers, dislocation sources operate in the microstrain region until the back stress from Orowan loops around the particles becomes large enough to stop the sources from operating. At this point the material has not yielded. Yield will occur

when particles are sheared by the loops, thus relieving the back stress and allowing the sources to operate again. This model gives the relationships

$$Y.S. \propto \frac{1}{\sqrt{d}} \quad \text{for a coarse dispersion}$$

$$Y.S. \propto \frac{1}{d} \quad \text{for a fine dispersion}$$

where d is the interparticle spacing. The results of several workers (27,28,37,40,50,51), some re-analyzed (45,46,48), agree with these relationships. However, several objections to this argument exist. One is that the stress necessary to shear an oxide particle is too high to be supported by the matrix, thus plastic flow around the particle or particle-matrix detachment should occur before a particle fractures. In addition, no fracture of incoherent particles other than large inclusions has been observed, although this is difficult to detect even with the aid of the electron microscope. A further objection to this theory has been raised by Abel and Ham (52) who found that in overaged Al-Cu single crystals the Baushinger effect increases with increasing pre-strain. Ansell and Lenel's model implies that the back stress, due to the particles, should not increase after yield has occurred since the particles are being fractured.

(iv) Several other workers have found empirical relationships between yield strength and the volume fraction of dispersed phase. Keeler found a direct proportionality as predicted by the law of mixtures for Zr-$ZrCr_2$ (53) and Zr-$ZrFe_2$ (54). Meiklejohn and Skoda found yield stress to be proportional to a complex function of volume fraction for iron particles

dispersed in mercury (51). Finally, Hibbard and Hart (55) found yield stress to be independent of volume fraction in overaged Cu-Co alloy.

On the basis of experimental agreement and mechanism the Orowan criterion seems to be the most likely. However, it is a two-dimensional model and neglects the possibility of cross-slip. Hirsch (56) has shown that a dislocation can cross-slip around a particle leaving behind a prismatic dislocation loop and creating a jog in the dislocation. If the dislocation is of screw character this cross-slip can result in a Frank-Read type dislocation source in the primary slip plane to which the cross-slip has occurred. The particles act as stress concentrators to supply the energy necessary for cross-slip. Prismatic loops and jogged dislocations have been observed by transmission electron microscopy (18,40,49,57,58). Cross-slip occurs at stresses lower than those necessary to force a dislocation between particles, thus if cross-slip is the yield criterion it should give a lower yield stress than that demanded by the Orowan model. However, the temperature dependence of flow should be greater than that of the elastic modulus if cross-slip controls the yield stress whereas in fact they are about the same (59,60).

Thus the yield stress is equal to the critical shear stress of the matrix plus the Orowan stress due to the forcing of dislocations between particles. In addition, there are two small contributions to the yield stress. One is due to elastic strains in the matrix caused by a difference in the coefficients of thermal expansion of the particle and the matrix when the alloy is cooled after heat treatment (18,61,62). The other is the result of a difference between the shear moduli of

the matrix and the particle (63). Both these effects cause the dislocations to "stand off" from the particles, thus decreasing the effective interparticle spacing. A typical value of this stand off distance is one tenth the particle radius (25). This value assumes that the shear modulus of the particle is greater than that of the matrix, as is generally the case.

2.3. Theories of Work Hardening.

Dispersion strengthened alloys generally work-harden much more rapidly than do the matrix materials without a dispersion. After several percent strain the rate of work hardening falls off, and the stress-strain curve becomes approximately parallel to that of the matrix alone (64,65). Fisher, Hart, and Pry (66) have developed a work hardening theory for these alloys based on Orowan loops left around particles. They postulated that the back stress exerted on dislocation sources by the loops is responsible for the work hardening, neglecting the contribution to the back stress from loops in parallel or intersecting planes. Hart (64) obtained reasonable agreement with the theory but other workers (37,55,67) found it necessary to modify the relationship to obtain agreement. Calculations reveal that more than thirty loops about each particle are necessary to cause the observed hardening (9) and the stress caused by thirty concentric loops is greater than the theoretical matrix shear stress. In addition, the observed temperature dependence of the flow stress is higher than that calculated from the theory (25,38,67,68). On these bases the theory must be rejected.

Ashby (25) has developed a work hardening theory based on the prismatic loops left when dislocations cross-slip past the dispersed particles. Single crystal experiments (37,60,69,70) show that these alloys exhibit multiple slip. Dislocation sources may be due directly to the presence of the dispersion as suggested by Hirsch (56). In addition a difference in coefficients of thermal expansion of the particles and the matrix can lead to dislocation creation (71-74) as can a difference in the elastic constants when a stress is applied (75). Thus interference between slip systems could occur leading to junction reactions between loops (76). These loops, which are often extended into dipoles under the influence of an applied stress, assume a lower energy cell structure. According to Ashby's theory the stress to force dislocations through this cell structure is the increment in flow stress caused by work hardening. Ashby supports his theory with the re-analyzed results of workers in Al-Cu (37,60), internally oxidized Cu (18) and Hg-Fe (51). The presence of the cell structure has been reported by numerous investigators (25,38,57,58,74,77,78) and it is a stable configuration. Thus it is a likely contributor to the work hardening behavior of these alloys. Mitchell, et al (24) have calculated that the thermally activated intersection of dislocations is the rate-controlling mechanism for deformation in overaged Al-Cu alloys. Their conclusion agrees with Ashby's that work hardening is due to the increased dislocation density. This is also supported by Barnby and Smith (78) who devised a model which predicts the strain at which a cell structure should have developed.

2.4. Other Considerations.

2.4.1 Stored Energy.

In those dispersion strengthened alloys which are produced by powder metallurgy, the extrusion process introduces energy into the structure as dislocation sub-boundaries (16,25,67,77,79) and also as elastic strain energy in the matrix and particles (16,17,80,81). This energy, most of which is retained after annealing since recrystallization is not common, makes a significant contribution to the strength and stability of the alloy (17,79-86). Preston and Grant (16) have devised a model which relates the strength of the alloy to the extent of the dispersion indirectly through its effect on the ability of the dislocation structure to retain strain energy. This model holds for internally oxidized copper but its validity in other systems has not been determined.

2.4.2 Preferred Orientation.

The extrusion process used in the manufacture of many dispersion strengthened alloys results in a preferred orientation of the matrix grains. SAP develops a $\langle 111 \rangle$ fibre texture (28) while thoriated nickel has a pronounced $\langle 100 \rangle$ fibre texture (87,88) which is stable even after annealing. It is interesting that SAP fibre texture is the same as that of pure aluminum, but thoriated nickel has a fibre texture while extruded pure nickel has no preferred orientation (19,87). The degree of development of the fibre texture in these alloys is determined by the extrusion ratio used in their manufacture.

2.4.3 Slip Lines.

Slip lines have been reported by several workers on overaged precipitation hardening alloys at tensile strains greater than 6 percent (25,69,70). They sometimes appear just prior to failure close to the fracture edge in the necked region. In these cases (6,59,69,70,89) they are indistinct and wavy, indicating that multiple slip is occurring. Other workers (37,41,60,90) report no slip line formation. There have been no slip line observations reported in oxide dispersion strengthened alloys.

2.4.4 Fracture.

Tensile fracture of overaged precipitation hardened alloys occurs either by necking in a ductile manner (37,90) or by cracking along an active set of slip planes (9,91). In SAP a dimpled fracture occurs in the centre of the specimen with micro-cleavage cracking around the edge (92,93). It is possible that cleavage cracks nucleate at the particle-matrix interface, particularly in oxide strengthened alloys where the particles are strong enough to allow a high stress to be generated at the interface during deformation (7). Particle-matrix interface effects may be responsible for the lack of ductility of many dispersion strengthened alloys (94-98).

2.5. TD Nickel

TD Nickel is a dispersion strengthened nickel alloy containing two volume percent thoria (ThO_2) (22,23,99). It is manufactured commercially by powder metallurgical techniques including compaction,

sintering and extrusion. The extrusion operation gives the alloy a strong <100> fibre texture and elongates the grains in the extrusion direction (57,87,100). This results in anisotropy of mechanical properties at temperatures above 300 degrees Centigrade (101). Strength and stability are developed by a series of strain-anneal cycles after extrusion. Thus the mechanical properties of TD Nickel are dependent on the dimensions of the (swaged) rod or (rolled) sheet. The final working is followed by a one hour stress relieving anneal at 1010 degrees Centigrade.

The spherical thoria particles are distributed evenly throughout the matrix with a mean spacing in the order of 1200 Angstroms. The size range of the particles is such that 86 per cent are less than 1000 Angstroms in diameter, the median size being about 500 Angstroms. No agglomeration of particles is evident even after annealing at close to 1400 degrees Centigrade (102).

The annealing behavior of this alloy is quite unusual. In the swaged condition it does not recrystallize (101) although a form of recovery occurs near 550 degrees Centigrade and also near 1100 degrees Centigrade. However, if TD Nickel is rolled, it does recrystallize when annealed above 500 degrees Centigrade (58,81,88,101). However, recrystallization does not drastically weaken this material (81,88,101) as is common in conventional metals and alloys.

Transmission electron microscopy reveals that in the extruded, stress relieved condition the alloy has a grain or sub-grain size of

about 1 micron diameter elongated to about 10 microns in the extrusion direction (58) with both large and small angle boundaries present. No elastic strain fields can be detected near particle-matrix interfaces (80). If a recrystallized specimen is deformed dislocations are inhibited by the particles, and cross-slip around them leaving prismatic loops (58). As deformation proceeds the heavy tangled dislocation structure which forms is gradually developed into a cell structure. This cell structure seems to be anchored by large thoria particles and thus has a cell size in the order of 3000 Angstroms.

Indications as to the actual strengthening mechanism come from two sources. Microstrain measurements on recrystallized TD Nickel indicate that strengthening is due to the formation of a deformation-resistant dislocation structure by the strain-anneal cycles (86). The thoria particles determine the fineness and stability of the dislocation network. This, however, does not explain the retention of strength after recrystallization when the dislocation structure has annealed out. Grierson and Bonis have shown (81) by Fourier analysis of broadened x-ray diffraction lines that deformation increases the elastic strain in the matrix. This increase is only partially relieved by annealing even when complete recrystallization occurs. Thus the particles seem to prevent the annealing out of elastic strains in the matrix. In swaged material strengthening is due to a combination of these two factors.

The creep fracture of TD Nickel has been studied by Wilcox and Clauer (100). They found that the fracture surface consists of two regions, one oriented at 45 degrees to the stress axis and one at 90

degrees. The 45 degree region has an intergranular appearance while the 90 degree region is covered with dimples similar to those caused by low temperature ductile fracture. Necking precedes this fracture and grain boundary voids are observed in the necked region. Wilcox and Clauer proposed that these voids originate with the detachment of grain boundary oxide particles. This could lead to shear of longitudinal boundaries with final rupture occurring when the voids merge. This explanation does not account for the different orientations of the two regions on the fracture surface, however, it does illustrate the complexity of the fracture behavior of TD Nickel.

CHAPTER 3

FATIGUE

This chapter deals with the fatigue behavior of face-centred cubic metals and alloys. Although there is no comprehensive, up-to-date review article on fatigue several older or more specialized reviews (103-108) are available.

3.1. Microstructure.

When an annealed metal or alloy is subjected to reversed cyclic stressing its initial response is to harden as total strain accumulates. This hardening, which is less than that which would result from an equivalent tensile strain (109,110), is accompanied by fine slip distributed at random throughout the specimen (109,111-115). Hardening decreases as cycling continues until it ceases or "saturates" after several percent of life at a stress which is a function of the plastic strain amplitude (112,116). At saturation slip becomes concentrated in irregularly spaced slip bands (111-114,116,117), typically ten to fifty microns wide and separated by fifty to several hundred microns. As cycling continues the slip bands become more numerous (113,114,116, 118) and more intense (112,118) particularly at high stresses. In polycrystals, some grains suffer heavy deformation while others show very little evidence of slip (112,119), thus slip bands do not usually cover more than 20 percent of the specimen surface. However, a high

density of slip bands usually appears adjacent to a growing fatigue crack (111,118,119) due to its stress-concentrating effect.

The slip lines which form during the rapid hardening stage may be removed by electropolishing a few microns of metal from the surface. However, once the slip bands have formed, electropolishing leaves dark traces on the surface where the slip bands have been removed (111, 118-120). These "persistent" slip bands are not removed until as much as one hundred microns is electropolished from the surface.

If a metal or alloy has been cold worked it softens during the early stages of fatigue (117,121-129) finally reaching a saturation level. High stacking fault energy metals saturate at a stress level which is independent of the initial condition of the specimen; however, low stacking fault energy alloys which have been cold worked saturate at a higher stress level than their annealed counterparts (130). Fully reversed stress is essential for fatigue softening (126,131). The slip bands formed in fatigue softening materials develop before saturation is reached and are more closely spaced than those in initially annealed metals (116,123,127).

The dislocation structure of fatigued specimens depends on stacking fault energy and the amplitude of the cyclic stress. Metals of high stacking fault energy when cycled at low stress (lives $>10^6$ cycles) exhibit a dislocation structure consisting of patches of high dislocation density several microns in extent and separated by relatively dislocation-free regions of similar size (115,132-135). These dense areas have a high concentration of small dislocation loops

and jogged dislocations. The boundaries of these patches are well defined and lie parallel to $\langle 111 \rangle$ directions (134). The dislocation loops are elongated in crystals undergoing single slip but are equiaxed under multiple slip conditions (133).

When cycled at high stress, these high stacking fault energy metals develop a cell structure during rapid hardening (112,115,132, 136-142). Cell formation is virtually complete at saturation and further cycling tends to thicken and rearrange the cell walls so that the cells become equiaxed (140). Cell boundaries lie in $\{111\}$, $\{110\}$ or $\{100\}$ planes and are made up of loops, tangles and jogged dislocations. In a polycrystal the substructure in adjacent grains may vary in its development from grain to grain depending on their orientations. There are indications that the presence of a non-zero mean stress is necessary for cell formation (115,140). Such a condition always exists in polycrystals due to grain boundary constraints. In general during fatigue the cyclic stress necessary to obtain a given dislocation configuration increases as stacking fault energy decreases (138). This may explain the failure of some workers (133) to observe a cell structure in fatigued copper.

Metals and alloys of low stacking fault energy when fatigued at high stress develop a structure similar to that obtained in high stacking fault energy metals at small stress amplitudes (142,143). However, if these materials are subjected to low cyclic stressing, dense two dimensional patches of jogged dislocations and loops appear

along slip planes or in faulted bands (115,133,134,144). These arrangements of dislocations correspond to the surface slip markings.

The rapid hardening stage of fatigue results from the creation of a dislocation structure which is determined by the stacking fault energy and the stress amplitude. An additional contribution to work hardening may arise from point defect generation. Saturation has been explained by two theories. One (116,145,146) considers the non-hardening strain to be due to annihilation of screw dislocations of opposite sign, thus permitting continued easy motion of dislocations in the regions where this has occurred. An alternative explanation due to Feltner (135) and valid in low stress fatigue ascribes saturation to the flip-flop motion of large numbers of the prismatic dislocation loops as the stress is reversed.

Forsyth (103,147) found evidence for the development of substructure in the persistent slip bands of aluminum alloys fatigued at low stress amplitude. This has recently been confirmed by transmission electron microscopy (148,149). The occurrence of the cell structure, which is present to a depth of one hundred microns beneath the surface, may contribute to the initiation of cracks in the persistent slip bands.

3.2. Initiation of Fatigue Cracks.

Fatigue cracks are initiated by the action of slip that is not fully reversed. The concentration of slip into slip bands gives the surface a characteristic notch-peak topography which often leads to cracking in the persistent slip bands (103,111,113,114,118,119,150-153).

There is a tendency particularly in alloys of low stacking fault energy for the persistent slip bands to form near twin or grain boundaries, thus cracks may be associated with these boundaries (111,118,119,143, 146,154-158).

Another phenomenon which affects crack initiation is the occurrence of extrusions and intrusions on the surfaces of many metals and alloys during fatigue (114,116,150,153-155,159-164). Extrusions are sheets of metal which extrude from slip bands at about the time that fatigue hardening saturates (155,156,162,165). Intrusions are grooves which appear at the same time, in some cases in the same slip band (155). Extrusions are typically 0.1 micron thick and 10 microns high although they are short and blocky in some alloys (150,155,161). They develop very quickly, growing as much as 50 Angstroms per cycle, however, growth usually stops within 100 cycles.

Since intrusions are primitive notches, it is not surprising that fatigue cracks are often observed in the vicinity of these features (153,162,166). Several theories have been developed to explain the formation of extrusions and intrusions (116,156,167-170), most of these based on cross-slip. This agrees with the observations that the formation of these features is enhanced in alloys of high stacking fault energy (113,114,116,157,158,169), fatigue lives being correspondingly shortened (114,143,146,169). Lowering the test temperature results in thinner extrusions which are more closely spaced than those which form at room temperature.

Many workers have observed pits in persistent slip bands (103,118,119,161,164). These may in fact be narrow intrusions or, as several investigators (164,171) have suggested, a consequence of subboundary cracking.

Slip bands and crack paths in cold worked and in annealed metals are similar (122); however, extrusions occur in cold worked specimens during the fatigue-softening stage (116) whereas in annealed material they do not generally appear until saturation.

That a free surface is necessary for crack initiation has been demonstrated by several experiments. If an anodic oxide film is formed on the specimen surface, the formation of slip bands, extrusions and cracks is suppressed as long as the film remains unbroken (114). The fatigue life of such a specimen can thus be extended apparently indefinitely. If slip lines are repeatedly polished away before they become concentrated in bands, or if persistent slip bands are completely polished away, the fatigue life is similarly prolonged (111,118). Annealing a specimen repeatedly before it reaches saturation also prevents slip intensification and extends the fatigue life (114) although once slip is concentrated in bands annealing has no effect (111,118,151).

There is considerable evidence to indicate that in high stacking fault energy metals, particularly at high stress ranges, cracks may form in sub-grain boundaries at the surface (143,171,172). Since these sub-boundaries lie in $\{111\}$ planes it is difficult to distinguish this type of initiation from normal slip band cracking. Sub-boundary cracking may originate with the formation of pores at sub-boundaries during high stress fatigue (164). Specimens which have been cold worked to develop a sub-structure are also susceptible to this type of failure.

Extrusions, intrusions, grain boundaries, twin boundaries and sub-boundaries all influence fatigue behavior although none of these factors is a prerequisite for failure.

3.3. Propagation of Fatigue Cracks.

The separation of the fatigue process into crack initiation and propagation is rather arbitrary. However, since cracks are usually present well before ten percent of the fatigue life, their behavior from that point is described as propagation. It has been found (163,173) that fatigue crack propagation in specimens stressed axially or in torsion occurs in two stages.

Stage I is slip plane fracture which occurs by an "unslipping" or reverse glide. This is an extension of the initiation process and is controlled by the range of resolved shear stress acting on the slip plane. The crack front may be sharply serrated with the tip acting as a dislocation source. The fracture path, since it follows active slip planes, deviates when it crosses a grain boundary thus giving the fracture surface a faceted appearance but the general fracture plane is one of maximum shear stress. In favourably oriented single crystals or in cold worked pure metals with a preferred orientation the Stage I process may continue to final fracture.

In most cases the crack grows a short distance into the interior of the specimen and then changes to a Stage II crack growing at right angles to the direction of maximum tensile stress. The conditions which favour this change are those which prevent easy glide including high stress amplitude, mean tensile stress, slip plane obstacles such as second phase particles, and the growth of the crack into the depths of the specimen where the shear stress/tensile stress ratio is low. Stage II growth is controlled by the value of the maximum principal tensile stress in the region of the crack tip.

When Stage II cracking predominates along the crack front the fracture is basically cleavage. However, as the crack grows the peak stress rises until microscopic plastic deformation occurs at the crack tip. It is at this point that the characteristic fatigue striations become resolvable on the fracture surface. Each striation results from one stress cycle, the spacing of the striations thus indicating the local crack growth rate (174).

Striations may be one of two types, brittle or ductile, depending on the environment, the stress conditions, and the mechanical properties of the material. Brittle striations lie on crystallographic planes which form facets at an angle to the general fracture plane. They do not normally appear except in a corrosive environment. Ductile striations lie on plateaus, the surfaces of which are parallel to the general fracture surface. The boundaries of the plateaus are, at least in some cases, grain boundaries.

As the crack grows longer, the tip stress rises, the striations become more heavily defined and cross-slip becomes extensive enough to turn the fracture path back to a plane at 45 degrees to the maximum tensile stress direction (163). This type of fracture is called shear decohesion failure. The stages of crack growth as described above are shown in Figure 1, although not in the proportions in which they occur in a specimen.

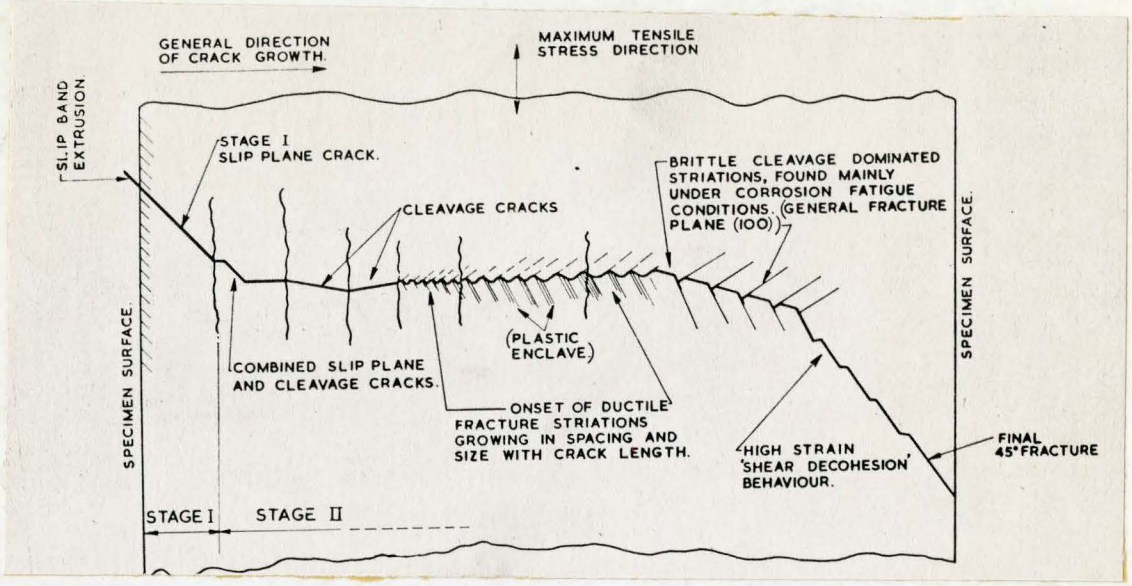

Figure 1

Stages of Fatigue Crack Propogation

Striations have been examined by optical and electron microscope studies of fracture surface replicas (175-178). On the basis of this work several explanations for the occurrence of striations have been proposed. Forsyth and Ryder (174) postulated that the hydrostatic stress operating ahead of a propagating crack opens up voids which are then linked to the crack by ductile rupture of the metal between. Laird and Smith (179) using the stress analysis of Williams (180) showed how "ears" can form at the tip of a crack as the stress changes from the compressive limit into the tensile half of the cycle. These ears are then folded as the crack closes and sharpens, thus leading to striations. McEvily and Boettner (157) have modified this mechanism to include the effect of crystallography. These workers have also explained the

ripples which sometimes occur between striations as being slip steps which form during the compressive half of the cycle (181).

According to Forsyth (163) a ductile striation forms in two steps, an easy slip component on a flat crystallographic plane followed by motion where the slip must conform to the curved crack fron by cross-slip. This latter step effectively blunts the crack tip so that resharpening by the compressive half of the cycle is necessary for further propagation. Forsyth also explains the appearance of the fracture surface in the high strain shear decohesion region. Striations are formed on this surface, however, the second step, involving cross-slip, dominates their formation thus shifting the orientation of the fracture surface.

The role of grain boundaries in transcrystalline fatigue crack propagation is uncertain. Crussard et al (176) have shown that grain boundaries do not affect the striations while Pelloux (177) has observed striations orientation changing at a grain boundary.

There is also some evidence to indicate that at high stress amplitudes substructure formation is important to fatigue crack propogation in materials with high stacking fault energies. Several workers (157,182,183) have found that the fracture surface of fatigued aluminum contains a highly developed substructure to a depth of less than fifty microns. This may be related to the cell structure observed in persistent slip bands or alternatively, the stress field at the tip of a growing crack may be sufficient to cause subgrain formation (103,138, 139,147,153,184-186). Since cross-slip is associated with the formation

of subgrains the observed dependence of crack growth rate on stacking fault energy may therefore be explained (143). It is likely that sub-boundaries act as dislocation sources, thus aiding propagation (138). Sub-boundary cracking is not inconsistant with the model of Laird and Smith (179) but does not fit Forsyth's striation theory. Grosskreutz (153) found in fatigued aluminum sheet that surface cracking (initiation) occurred along slip planes while in the interior the crack followed sub-boundaries. This may be a reasonable explanation for the high stress fatigue crack behavior of high stacking fault energy metals.

Under certain conditions, namely high stress and high homologous temperature, intergranular fatigue cracking can also occur. This effect has been reported in tin (187), silver chloride (188), α-brass (177), copper (125) and aluminum (119,181,189). Low cycling frequency enhances this effect (108).

3.4. Fatigue of Dispersion Strengthened Alloys.

The fatigue behavior of dispersion strengthened alloys has not been intensively investigated from a fundamental point of view although some studies have been made on overaged precipitation-hardened alloys. These alloys fatigue harden to a peak, and then gradually soften with further cycles until cracking occurs (52,190). Both single crystals (52,190) and polycrystals (191,192) exhibit a pronounced Bauschinger effect, particularly at low temperatures. Extrusions are not usually formed and slip intensification is not as rapid as in single phase alloys. The dislocation structure is characterized by tangles in the vicinity

of precipitates (190,193). Cracks may start from large fractured inclusions (158,177,181,194-197) or from grain boundaries (198), particularly at high stress amplitudes. Transcrystalline fractures are of the rough, shear type with the fracture plane lying at about 45 degrees to the direction of maximum tensile stress (190,199).

In steels, the initiation of fatigue fracture at cracked nonmetallic inclusions is well documented (200-203). Similar cracking of second phase particles in Udimet 700 has also been reported (204). In normal dispersion strengthened alloys such cracking is not likely since the second phase particles are small and usually equiaxed.

If the particles do not crack their effect on the rate of fatigue crack propogation depends on the width of the plastic zone at the crack tip (197). If the width of this zone is small compared with the interparticle spacing, then cracking is controlled by the matrix properties, with the particles effectively acting as crack arresters (195). In this case the growth rate as determined by striation spacings is larger than the macroscopic growth rate. However, if the interparticle spacing is much larger than the width of the plastic zone then crack growth is controlled by cracking around the particles (173), so that the macroscopic growth rate exceeds the microscopic rate.

For the case of oxide strengthened alloys the only fundamental fatigue study has been carried out by Martin and Smith (205). They found that in polycrystalline copper alloys internal oxidation reduced the fatigue life by promoting intergranular fracture. This effect is likely caused by the presence of oxide particles at grain boundaries.

The fatigue resistance of single crystals was improved by the oxidation, particularly when the oxide dispersion was very fine. Slip lines formed during fatigue, however, intensification was slow. The fracture path in both single and polycrystals lay at 45 degrees to the stress axis.

Several other investigators (2,3,4,13,23,199,206) have reported fatigue lives of SAP at various stress levels and temperatures. Their results are summarized in Figures 2 and 3. The trend toward higher fatigue ratios at high temperature is an indication that fatigue fracture of SAP is not intergranular, since high temperatures would encourage this type of failure (206). The detachment of particles from the matrix remains a possible contributor to fatigue failure in these alloys.

Figure 2. Fatigue Ratios of SAP

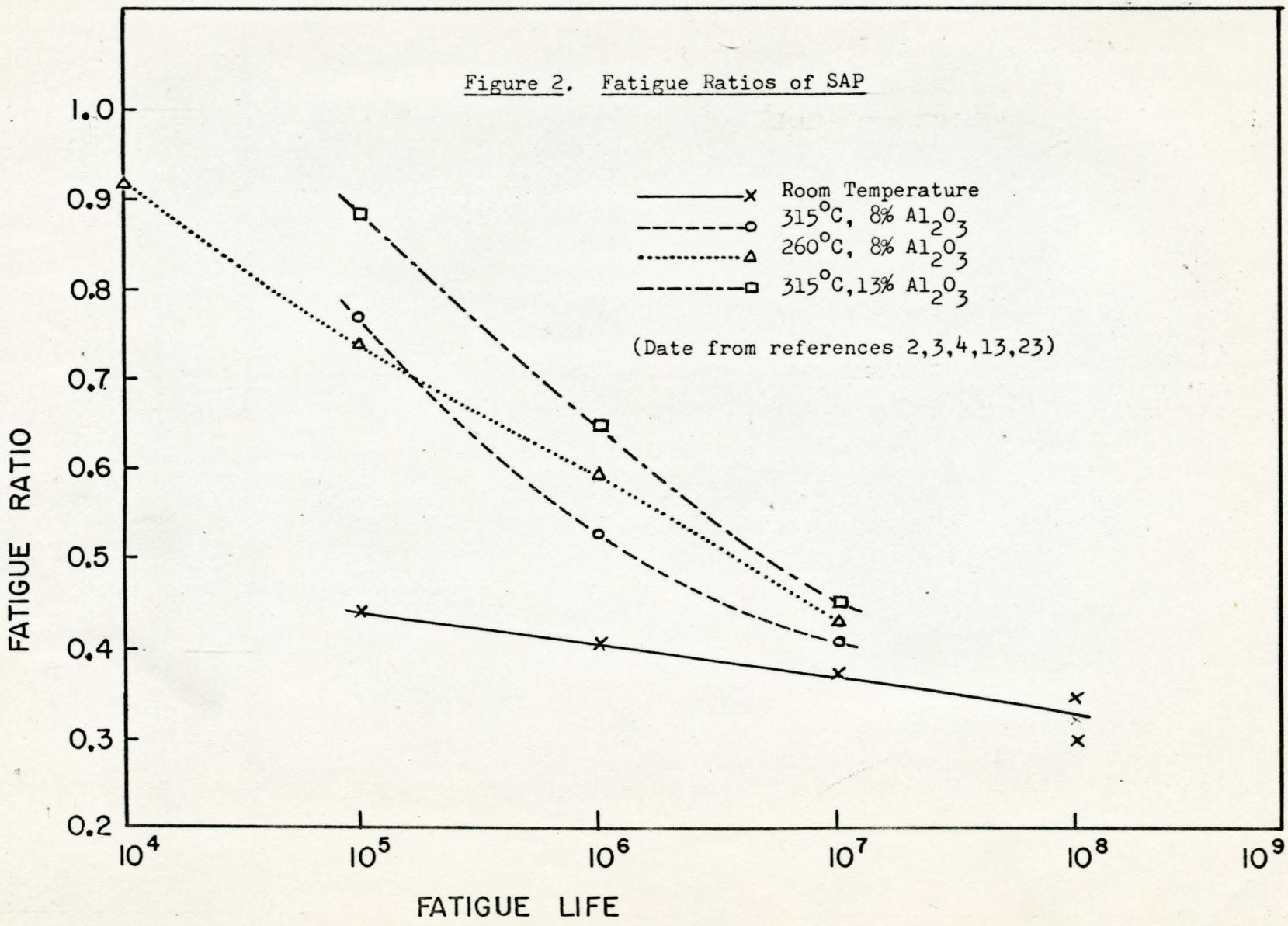

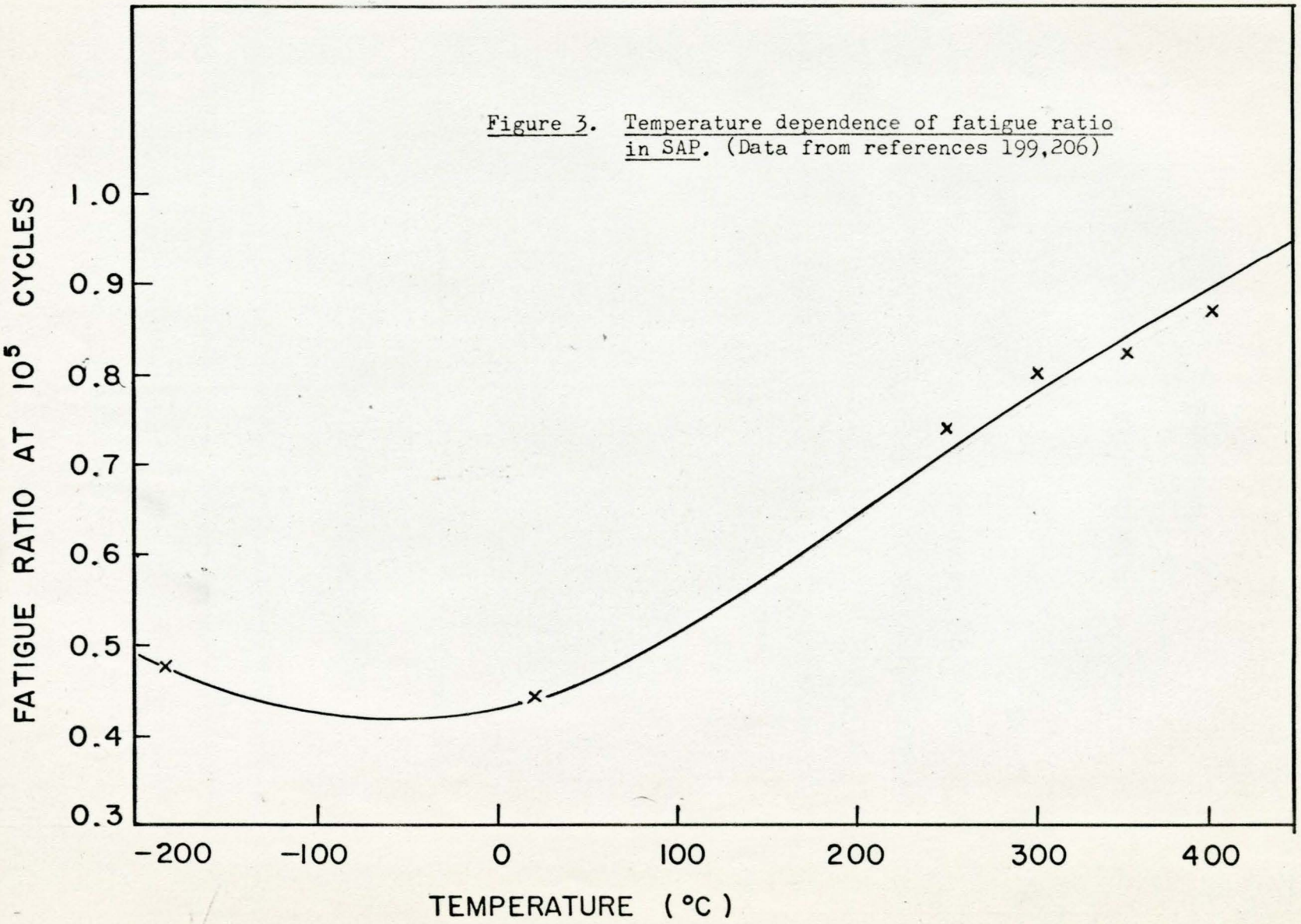

Figure 3. Temperature dependence of fatigue ratio in SAP. (Data from references 199,206)

CHAPTER 4

EXPERIMENTAL PROCEDURE

(i) Specimen Preparation.

TD Nickel was obtained from the Driver-Harris Company as 3/8 inch diameter rod. This material had been extruded, swaged, straightened and annealed at 1010°C for one hour. Fatigue specimens were produced by grinding gauge sections on the rod as shown in Figure 4.

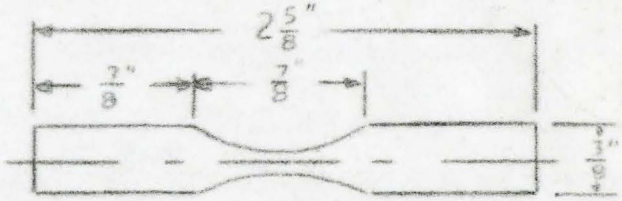

Figure 4. Specimen Configuration

The minimum diameters of the gauge sections ranged between 0.096 in. and 0.135 in. Several additional specimens were ground to a diameter of 0.135 in. along a gauge length of 0.85 in. These were used for

tensile tests. All specimens were electropolished prior to testing. This was done by masking the shoulders with Microstop lacquer and polishing in a solution of 40% H_3PO_4, 35% H_2SO_4, 25% H_2O at room temperature using a stainless steel cathode. After electropolishing the specimens were rinsed in distilled water and in methanol.

(ii) Mechanical Testing.

All fatigue tests were carried out under fully reversed, axial stress conditions (push-pull). Tests lasting longer than 10^6 cycles were performed at 1800 cycles per minute in a Sonntag SF-1-U fatigue machine with constant load amplitude. This machine was equipped with an oscilloscope connected to a linear variable differential transformer in order to monitor the strain values. By this technique a zero mean strain could be maintained throughout each test. The specimen surface was examined periodically with a low powered optical microscope. When a fatigue crack had grown around one-quarter of the specimen circumference the test was discontinued.

Tests at high stress amplitude were carried out in an Instron TTC-L precision tester modified for fatigue by Mr. D. F. Watt as described elsewhere (190). After electropolishing, specimens were mounted in precise conical grips and aligned in a jig to eliminate non-axiality. Constant load and constant total strain amplitude tests were performed at frequencies of 16 and 26 cycles per minute respectively. A continuous record of the test conditions was obtained on a recorder which plotted load against crosshead position. When cycling between

fixed load limits, the test was stopped after a crack had grown around one-quarter of the specimen circumference. When strain cycling the presence of a fatigue crack was indicated by an asymmetry of the peak stresses, the peak tensile stress dropping rapidly as the crack grew. The test was discontinued when the peak tensile stress had fallen to about half its initial value. This corresponded to a crack across more than three-quarters of the cross-section.

Several lengths of as-received rod were cold-rolled to a thickness of 0.005 in., annealed for 1 hour at 1000°C in argon, and pulled in tension to failure in a Hounsfield Tensometer. Tensile tests were also performed on bulk specimens using a Tinius Olsen tensile machine.

(iii) Specimen Examination.

Fatigue specimens in the cracked condition were examined with a Reichert optical microscope to determine the positions of fatigue cracks with respect to surface features. The specimens were then subjected to further examination by other techniques.

Thin film transmission electron microscopy.

From as-received and fatigued specimens, thin slices were spark cut with a moving Mo. wire on a Servomet spark cutter. This apparatus is described in more detail in Appendix A. These slices, which were 0.005 to 0.015 in. thick were cut either perpendicular to the specimen axis, parallel to the specimen axis or parallel to the fatigue crack. Since the specimens had non-uniform cross-sections, each slice had been subjected to a different fatigue stress amplitude. It

was therefore necessary to accurately measure the diameter of each slice at this stage. The slices were then cleaned in a solution of 50% CH_3COOH, 30% HNO_3, 10% H_2SO_4, 10% H_3PO_4 at 85°C to remove the carbon layer deposited during the spark cutting. They were then electropolished by the window method in 40% H_3PO_4, 35% H_2SO_4, 25% H_2O at -20°C with a current density of 2-3 amps/cm^2. Thin films obtained by this method were examined in a Siemens Elmishop I electron microscope at 100 kV.

Bulk tensile specimens which had been pulled past the ultimate tensile stress were sliced through their necked regions. The slices were cleaned and electropolished as described above for electron microscope observations. In addition, thin films from near the fracture of the rolled and annealed foil were examined in the electron microscope.

Electron fractography.

Fatigued specimens containing cracks were pulled to failure in the Tinius Olsen tensile machine. The fracture surfaces thus obtained were replicated by a two step process using parlodion and a 50-50 platinum-carbon mixture. The latter was evaporated onto the parlodion in a vacuum at a shadowing angle of 40°. Replicas obtained in this fashion were examined in the electron microscope at 80 kV.

Optical Microscopy.

The fatigue and tensile fracture surfaces were also examined with the Reichert optical microscope. This was accomplished by direct observation as well as by the examination of celluloid replicas stripped

from the fracture surface and shadowed with aluminum.

The propagation of cracks was studied by sectioning cracked specimens parallel to the specimen axis in a plane perpendicular to the plane of the crack. These sections were mounted in bakelite, polished and etched with Carapella's Reagent (99 ml. C_2H_5OH, 2 ml. HCl, 5 g. $FeCl_3$). They were then examined using the Reichert microscope.

X-Ray.

A specimen of as-received TD Nickel was electropolished to a point and exposed to unfiltered Cu radiation in a transmission Laue configuration to determine the degree of preferred orientation. In addition, an Acton (Cameca) electron probe microanalyser was employed to determine the extent of impurity segregation, if any, in the material.

CHAPTER 5

RESULTS

The use of the two testing machines made it possible to cycle at low stress quickly and at high stress precisely. The experimentally determined S-N curve is shown in Figure 5 including the data given by Anders et al (23).

When load cycling in the Instron at high stress, cyclic creep was observed. This was manifest as the gradual necking of the specimens followed by double-cup fracture at lives much shorter than indicated by the S-N curve. Cyclic creep was not observed when load cycling at low stress or when strain cycling at high stress.

The most meaningful results were obtained by cycling at high stress between constant total strain limits. In these tests the peak stresses were observed to drop for the first few thousand cycles, finally reaching saturation at about 70% of the fatigue life (Figure 6).

Despite the fact that specimens were electropolished before testing, surface irregularities such as polishing pits were often present. These marks were usually the sites of the first observable fatigue cracks. The fatigue cracks propagated at an angle of about 45° to the specimen axis regardless of whether or not they initiated at surface marks.

During the final 50 to 100 cycles of each strain-controlled test, which were applied at a frequency of about 1 per minute, an irregularity developed in the compressive halves of the cycles, as shown by the arrows in Figure 7. This irregularity occurred at lower compressive loads and became more pronounced as the specimen approached final fracture.

The tensile tests revealed that the material had an ultimate tensile strength of 100,000 psi. and showed a deviation from elastic behavior at 72,000 psi. Tensile fracture occurs at 17% elongation with a reduction in area of 82%.

Transmission Electron Microscopy.

The structure of the as-received material is shown in Figure 8. The distributions of thoria particles and grain boundaries can be clearly seen. Some but not all of the boundaries contain thoria particles. The grains are .2 to .5 u in size and relatively free from dislocations except in the boundary regions. Selected area diffraction was attempted to determine the misorientation of these grains, however, this proved in most cases to be impossible since the grain size was so small that each diffraction pattern contained spots from several grains. However, a few successful determinations were carried out, these revealing boundary angles ranging from 8° to 20°. For the purposes of this work, they will be referred to as grains regardless of the boundary angle.

Figure 9 shows the structure after 1,357,000 cycles at ±47,000 psi. An increase in dislocation density both at the boundaries and inside the grains is evident. There is no change in grain size and no evidence of particle-matrix detachment.

The structure in a plane parallel to the specimen axis after 6800 cycles at ±88,000 psi. is shown in Figure 10. The thoria particles are stringered to some extent in the extrusion direction and are frequently associated with grain boundaries. Dislocations are present in the interiors of some grains. The grains are .2 to .5 u wide with lengths in the order of 5 u. There are no indications of particle-matrix detachment.

Figure 11 is a thin film taken from near the fracture of the rolled, annealed foil which was pulled to failure in tension. The grain boundaries have been removed by the annealing treatment. Interactions between dislocations and thoria particles can be clearly seen but there is no sign of particle-matrix separation.

The structure of the material in the necked region of a bulk tensile specimen is shown in Figure 12. The dislocation density in the interior of the grains is higher than in the fatigued specimens. The grain size, however, has not changed. Once again there is no visible particle-matrix detachment.

In all thin films, some clustering of thoria particles was evident. These clusters were spaced approximately 0.5 u apart and were stringered in the extrusion direction.

Electron Fractography

Fracture surface replicas showed that on a submicroscopic scale the high stress (short life) fatigue fracture surfaces contained many different features. Several types of features are shown in Figure 13. Myriads of fine "pin-head" specks in the order of 50 A° diameter can be seen. These are considered to be coagulated shadowing

material. In addition there are a number of small craters in the replica (bumps in the fracture surface), these being 1000-2000 A° in diameter. Surface disturbances on a larger scale are visible. These appear to be ridges on the replica (crevices in the metal surface) in that they cast shadows on the replica surface. The ridges are often curved as if to partially enclose a structural unit .5 to 3 u in size. The third feature observed in this figure is a general linear texture running from the upper left to the lower right of the micrograph. This is more clearly shown in Figure 14. The lines are sometimes but not always parallel to straight segments of the surface ridges. Some surface areas seemed to consist of ledges separated by torn "cliff" edges. Such a structure is shown in Figure 15.

Occasionally a large surface structural unit was defined by the surface ridges. Examples of this are shown in Figures 16 and 17. In Figure 16 the line texture appears to be affected by the presence of this division. There is also a marked change in the density of the small craters. In Figure 17 a boundary separates a region containing two types of crater from a region which has a very rough appearance. This latter region is shown at higher magnification in Figure 18. It consists of craters and ridges with a definite orientation as if this surface had been dragged across another.

Two other features appeared occasionally on fracture surface replicas. One was a series of parallel straight lines or grooves across the surface as shown in Figure 19. The other was what appears to be normal Stage II fatigue striations, as shown in Figure 20.

Every series of striations terminated at a surface ridge, as shown in the figure, and the striation spacing always increased as they approached the ridge. The individual striations were less than 5 μ long. These striations, however, were not a common surface feature.

Optical Microscopy.

The surfaces of strain cycled specimens developed slip bands visible to the naked eye at about the time saturation occurred. These slip bands did not appear during load cycling at either high or low stress amplitudes. The slip bands always formed at about 45° to the specimen axis and the fatigue cracks grew along these bands. Figure 21 shows cracks initiated at polishing pits growing along the slip bands. Occasionally the crack turned through 90° and grew back toward the region of minimum cross-section as shown in Figure 22. This figure also shows the crack jumping between parallel slip bands, a type of behavior which was quite common. An increase in the concentration and intensity of slip bands near the crack tip was also observed.

Optical micrographs of the high stress (short life) fatigue fracture surfaces are shown in Figures 23-26. These surfaces were rough and often contained fissures (Figure 23), particularly near the specimen edge. Rows of striations covered the fracture surface (Figures 24 and 25). The striations lay perpendicular to the general direction of crack propagation (parallel to the crack front) and were spaced 15 μ to 25 μ apart.

The fatigue fracture surface also contained regions which were smooth except for straight parallel lines. These regions, which were always located adjacent to the area where final tensile fracture occurred, are shown in Figure 26.

The structure of the as-received material as revealed by sectioning, polishing and etching is shown in Figure 27. The widths of the elongated grains average about 1 μ. The lengths of these grains are difficult to estimate as it is virtually impossible to locate the grain ends even at high magnification. The inclusion-like objects shown in Figure 27 were located randomly throughout the structure although not in large numbers. Microprobe analysis of these objects showed that no foreign elements were present and the back-scattered electron image suggested that they were in fact voids.

Cross-sections of the specimens containing cracks are shown in Figures 28-31. In all cases the sections were cut in a plane at right angles to the plane of the crack. The micrographs shown are from specimens which failed under high stress conditions and the directions of crack growth are from left to right on the micrographs. Figure 28 shows a typical fatigue crack in the interior of a specimen, running at 40 to 50° to the specimen axis. The small sub-cracks growing at an angle to the main crack were present in all specimens and were generally spaced 10 to 50 μ apart. These sub-cracks are shown at higher magnification in Figure 29. It can be seen that the sub-cracks are branched and do not grow parallel to the direction of elongated grains. Figure 30 shows a crack which exhibited a great deal of branching with one branch in the process of rejoining the main fracture. The figure also shows the elongated voids mentioned above. These voids occasionally linked up with the crack (Figure 31) but only when the crack grew very close to them. In all these figures there is a noticeable distortion of the elongated grains around the crack.

Tensile Specimens

The fracture surfaces of bulk tensile specimens contained cross-shaped fissures as shown in Figure 32. When the arms of the cross were not mutually perpendicular, an additional fissure sometimes formed in one of the larger uncracked segments. In all cases the arms of the cross were within 20° of being mutually perpendicular. One tensile specimen which had been pulled past its ultimate tensile strength to 10% reduction in area was sectioned through the necked region perpendicular to the specimen axis. No cracks were observed in this specimen.

One of the tensile specimens necked down unevenly so that at one point the edge of the fracture surface was tangential to the circumference of the original cross-section. The fracture surface of this specimen is shown in Figure 33.

Figure 34 and 35 show polished and etched sections cut parallel to the axis of a tensile specimen so as to include the necked region. It can be seen that the regular elongated grain structure has been distorted in the tensile neck, and the elongated voids are no longer evident. Instead there is a high concentration of smaller voids, averaging about 10 μ to 25 μ in size. Figure 35 shows the root of the cross-shaped crack. The crack follows a path which includes these voids but it does not appear to be intergranular.

All these tensile results are for bulk specimens, that is, specimens with a circular cross-section. In addition, rolled sheet specimens were pulled in tension to failure. When the sheet was in the order of 0.025 in. thick, fracture occurred in a plane at about 50°

to the stress axis as seen on the broad side of the specimen. This type of fracture was accompanied by necking such that the thickness, but not the width of the sheet was reduced. The fracture appeared to be a shear failure with the shear occurring in the direction in which no necking had occurred.

X-Ray Investigation

The x-ray studies showed that the TD Nickel had a pronounced ⟨100⟩ fibre texture (Figure 36). This texture was so well developed that the angular spreads of the arcs on the x-ray film were less than 5°, corresponding to a spread in grain orientation of about 2° about the ⟨100⟩ direction.

Figure 5. S-N curve for TD Nickel

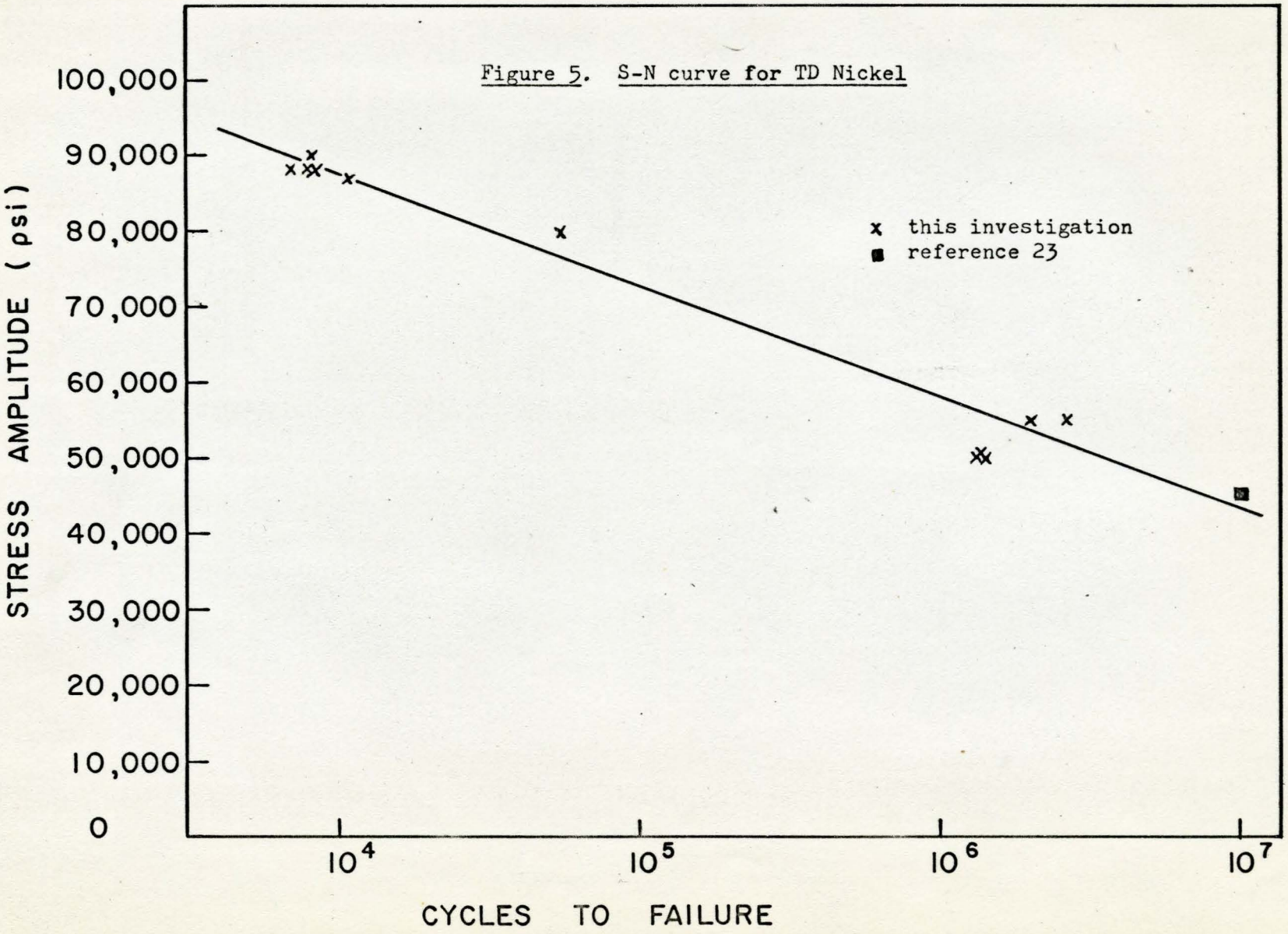

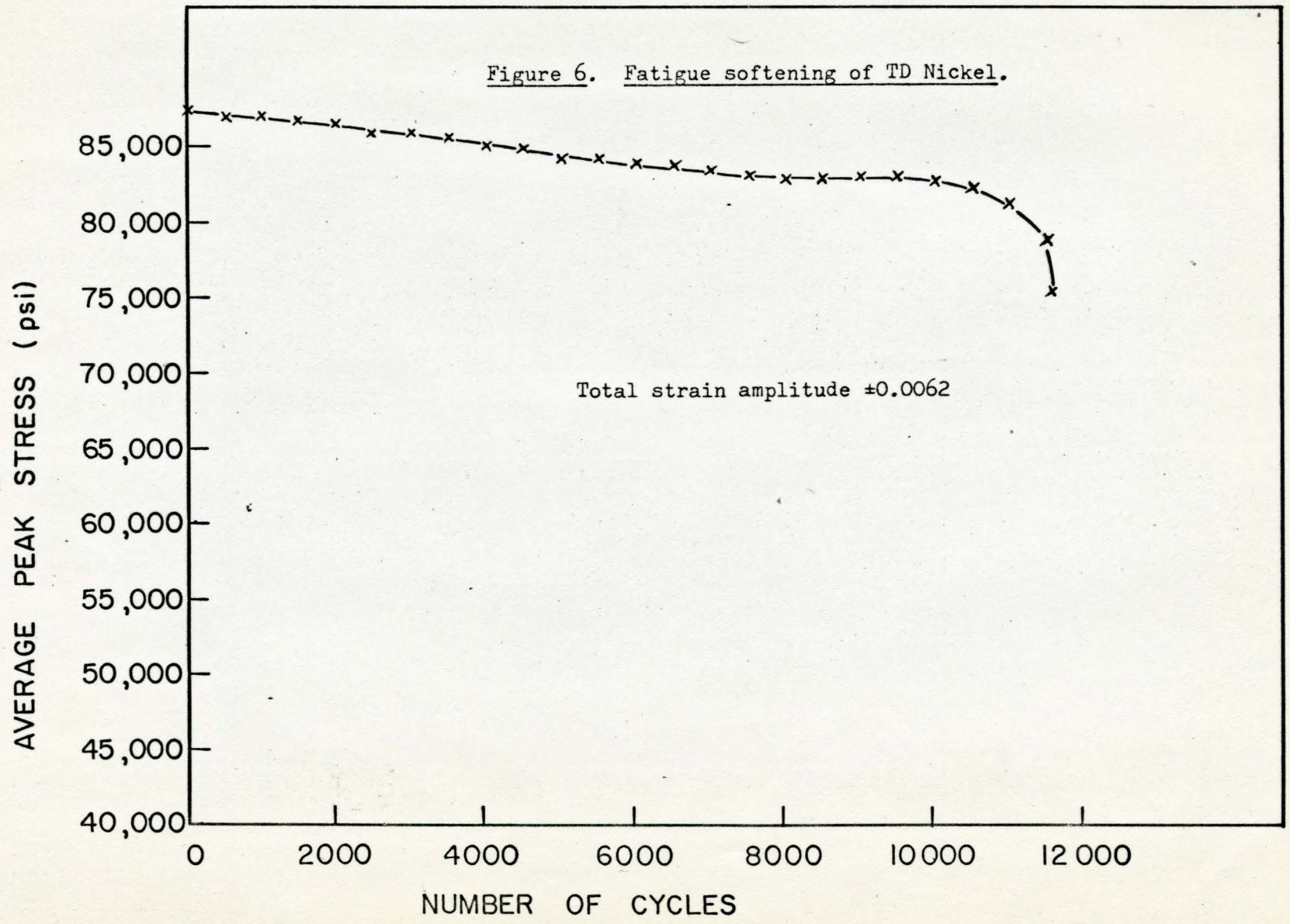

Figure 6. Fatigue softening of TD Nickel.

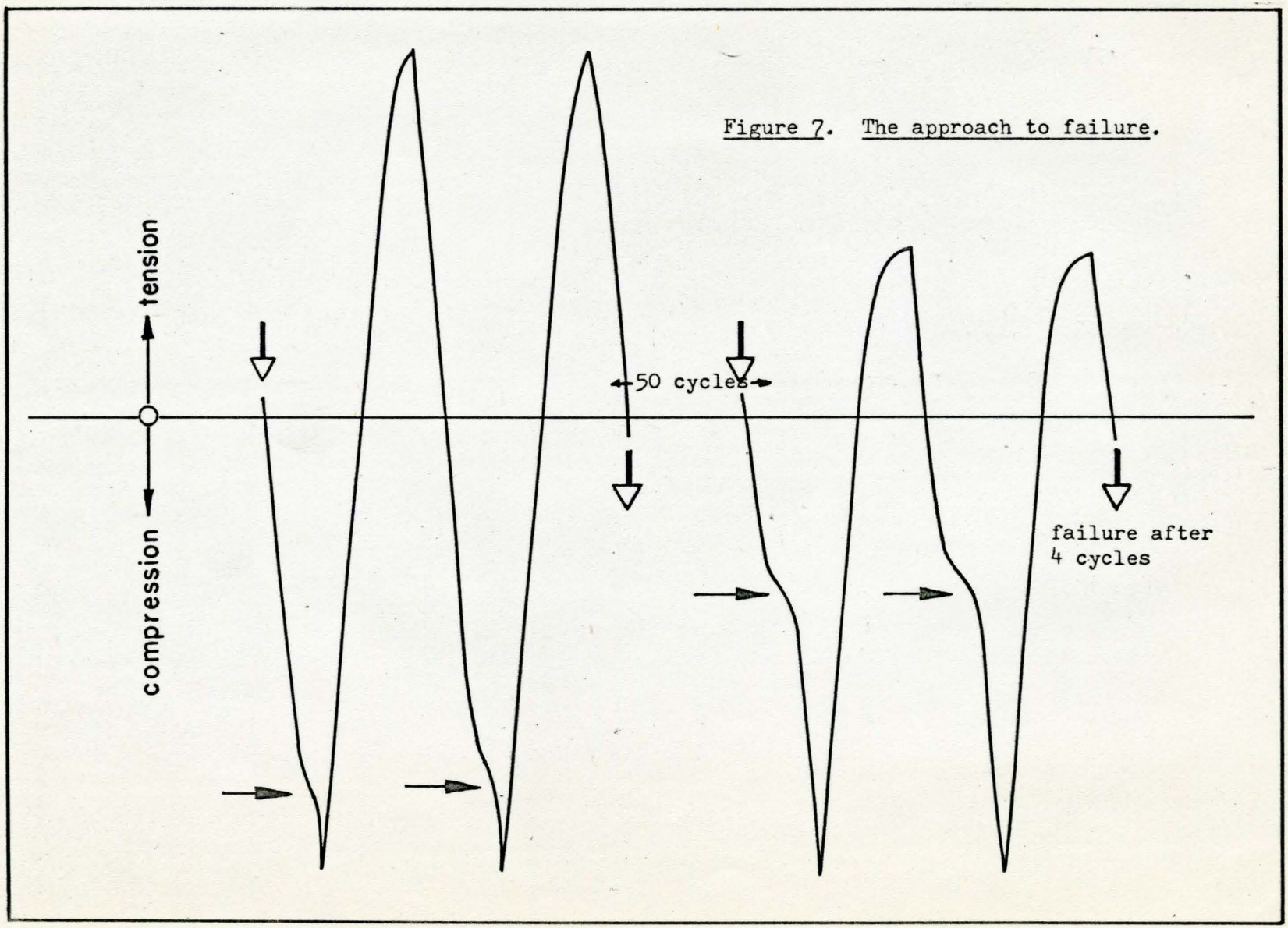

Figure 7. The approach to failure.

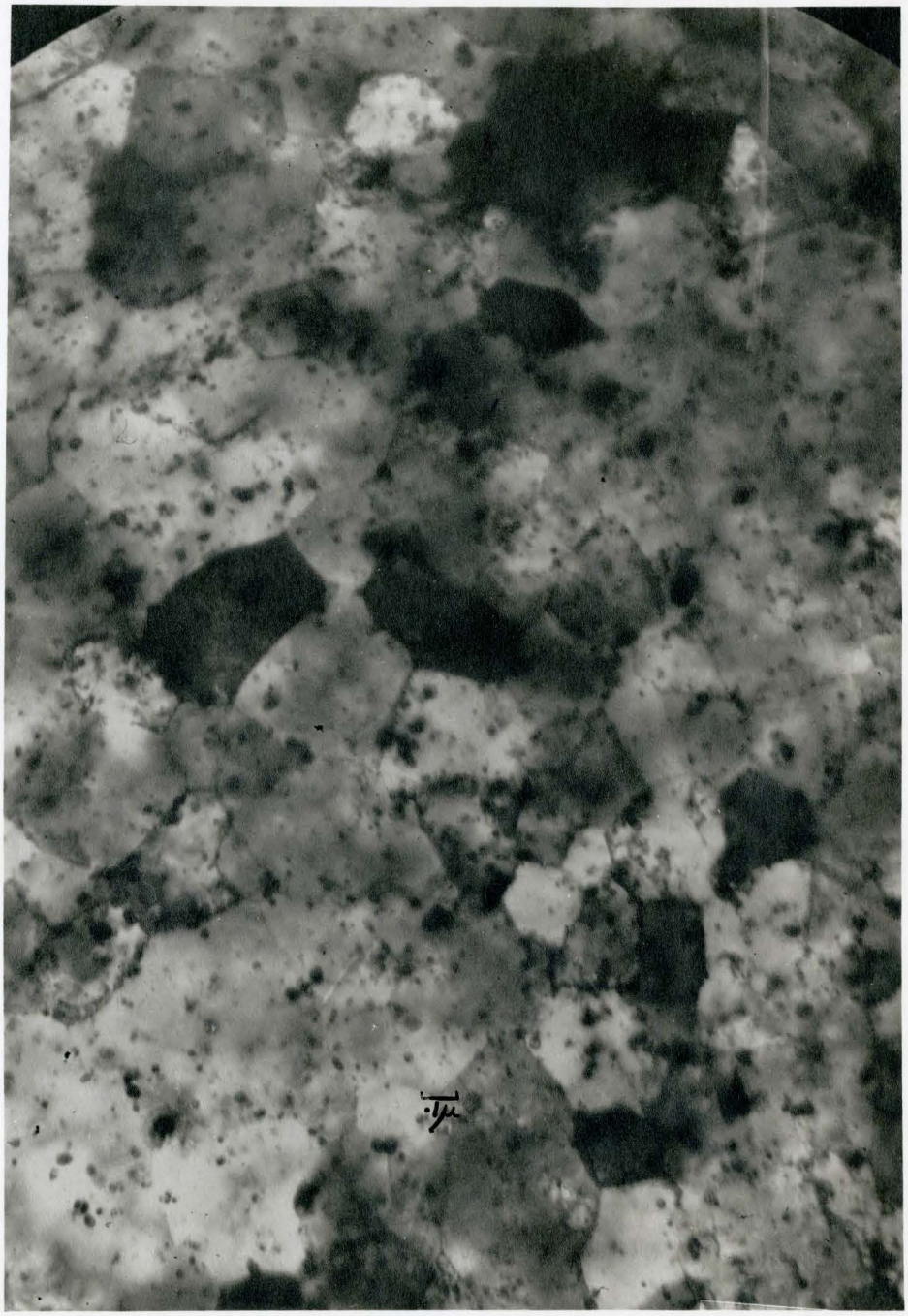

Figure 8. As received TD Nickel.
Electron Micrograph from a thin film cut perpendicular to the specimen axis.

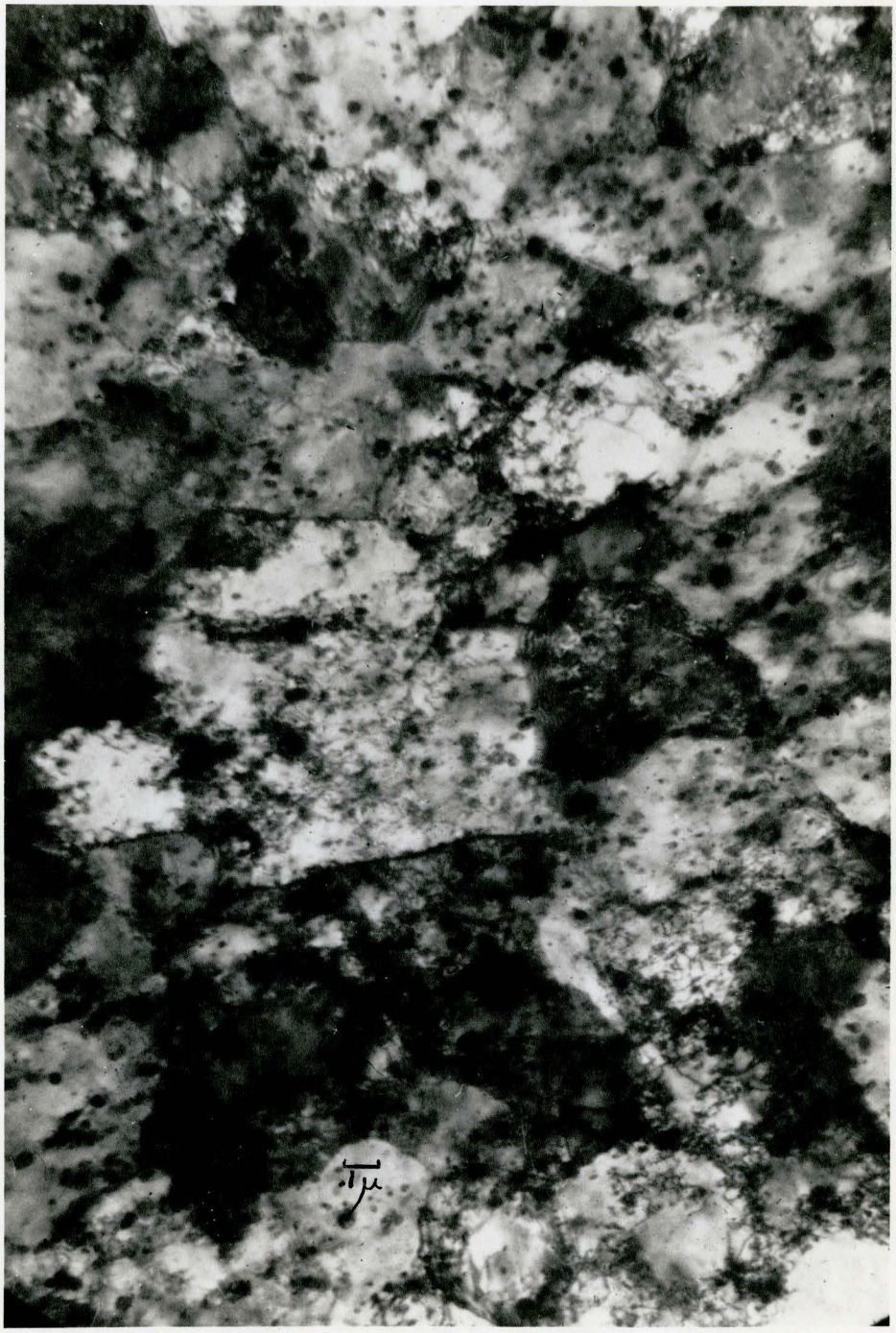

Figure 9. TD Nickel after 1,350,000 cycles at ±47,000 psi. Electron Micrograph from a thin film cut parallel to a fatigue crack (at 45° to the specimen axis.)

Figure 10. TD Nickel after 6,800 cycles at ±88,000 psi. Electron Micrograph from a thin film cut parallel to the specimen axis.

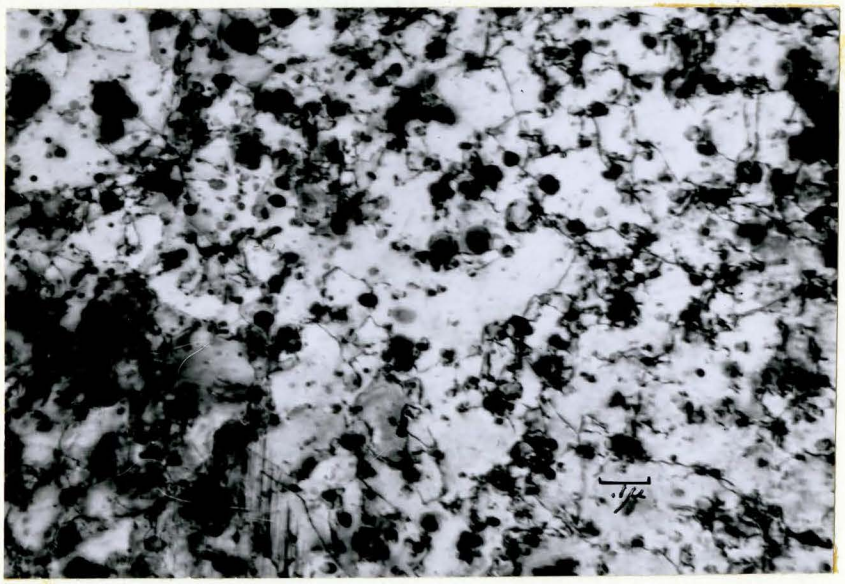

Figure 11. TD Nickel foil pulled in tension to failure.

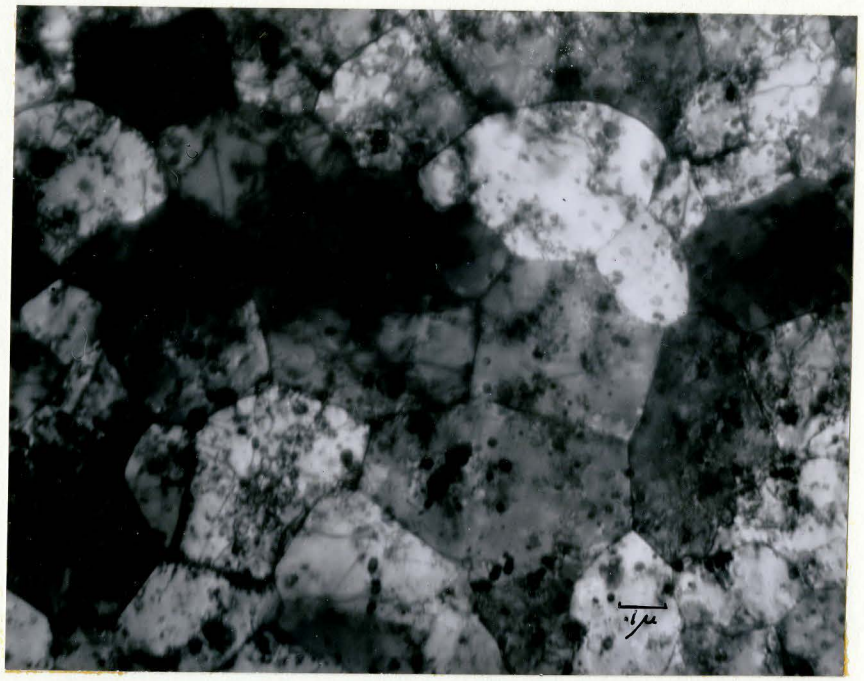

Figure 12. TD Nickel pulled in tension to 10% R.A. Electron Micrograph from a thin foil cut through the tensile neck.

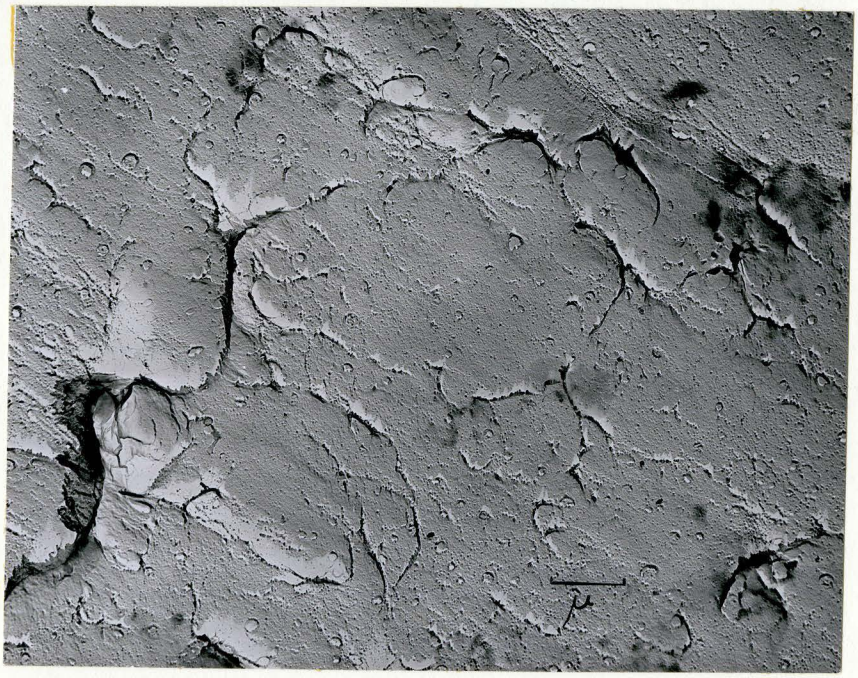

Figure 13. Electron Fractograph of fatigue fracture surface.

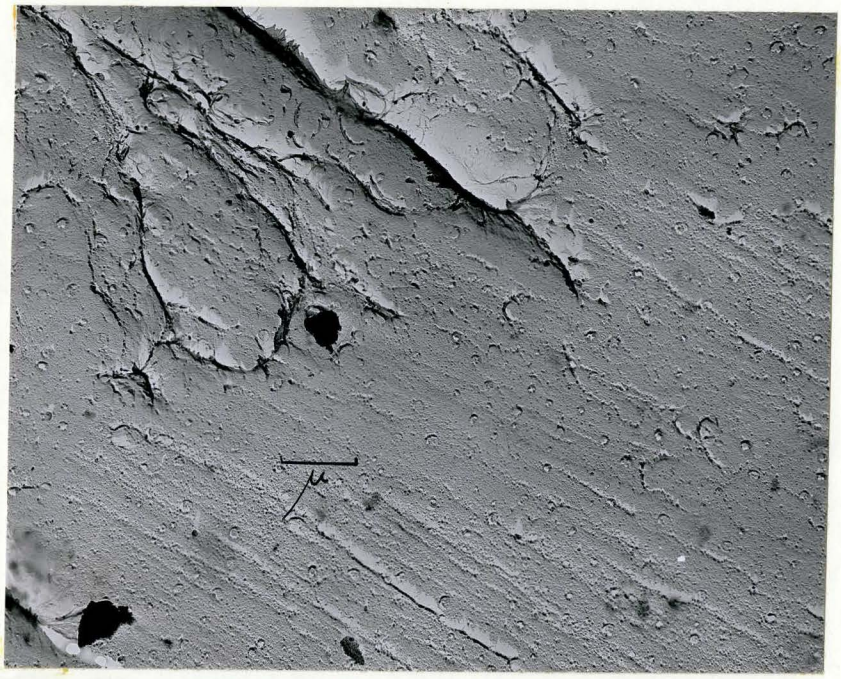

Figure 14. Electron fractograph of fatigue fracture surface.

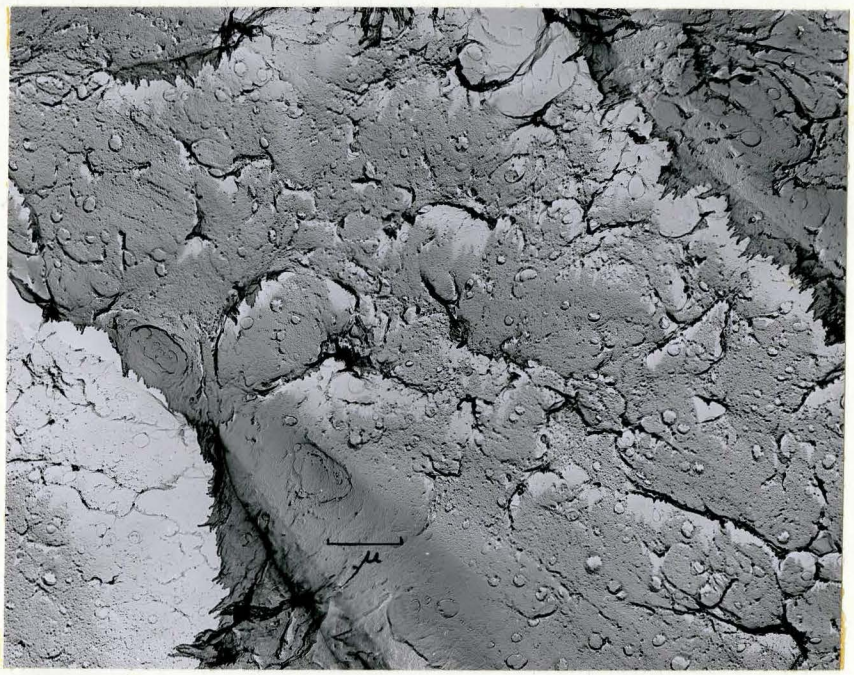

Figure 15. Electron fractograph of fatigue fracture surface.

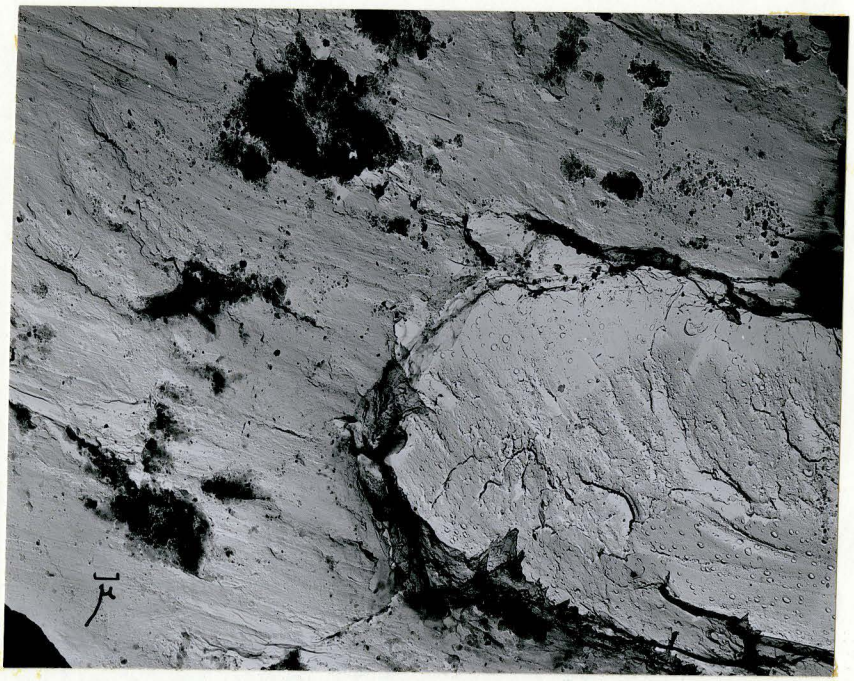

Figure 16. Electron fractograph of fatigue fracture surface.

Figure 17. Electron fractograph of fatigue fracture surface.

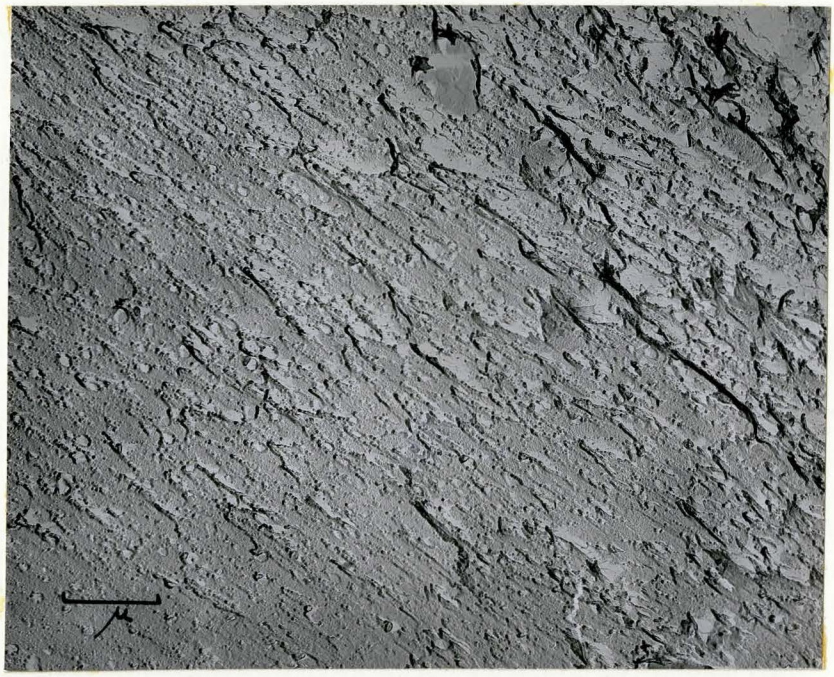

Figure 18. Electron fractograph of fatigue fracture surface.

Figure 19. Electron fractograph of fatigue fracture surface.

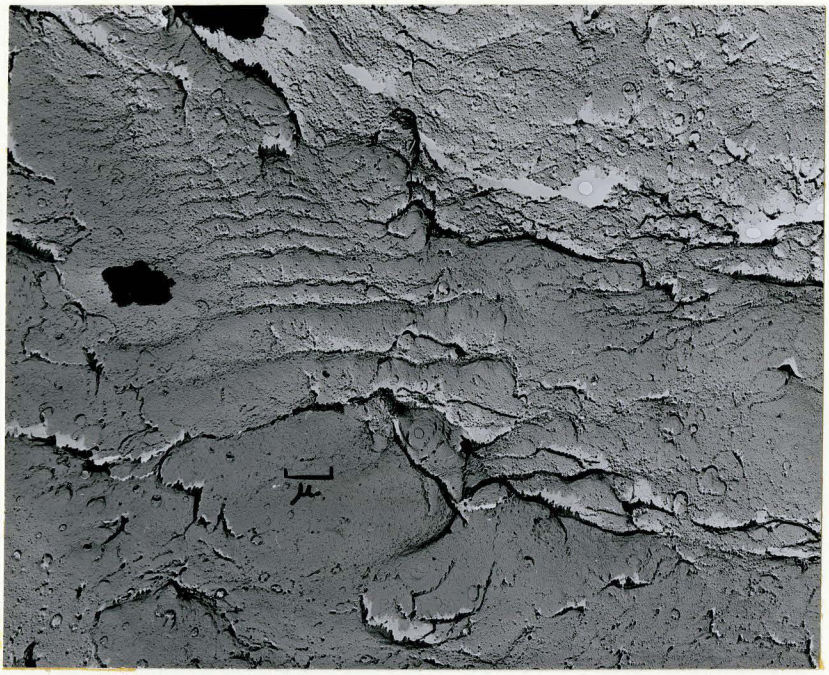

Figure 20. Electron fractograph of fatigue fracture surface.

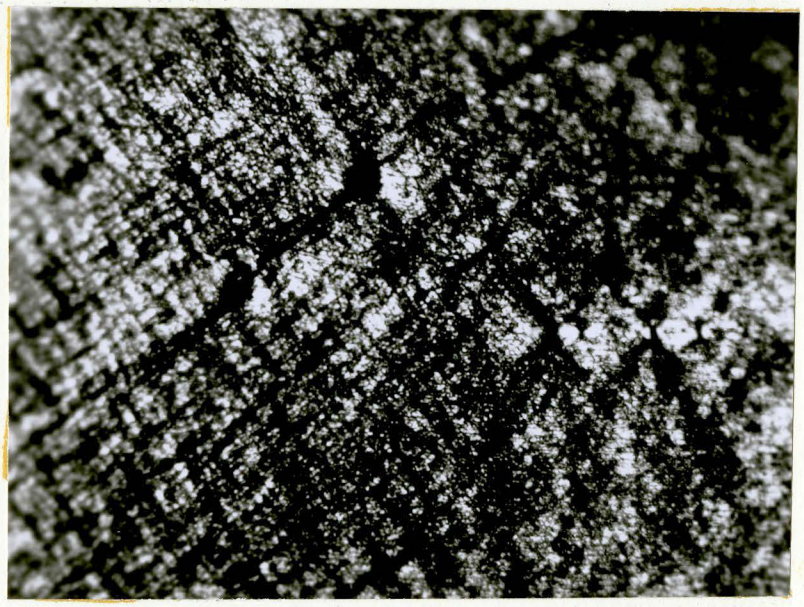

Figure 21. Fatigue cracks on specimen surface. 220 x
Specimen axis horizontal.

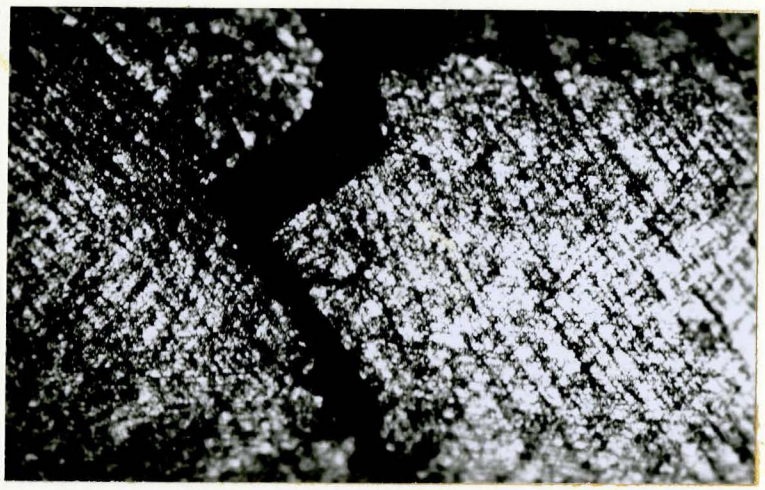

Figure 22. Fatigue cracks on specimen surface. 120 x
Specimen axis horizontal.

Figure 23. Optical micrograph of fatigue fracture surface.
85 x

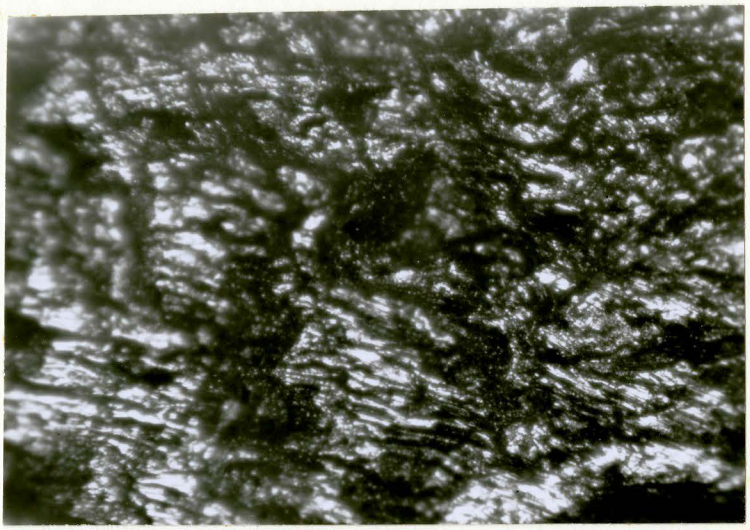

Figure 24. Optical micrograph of fatigue fracture surface. 120 x

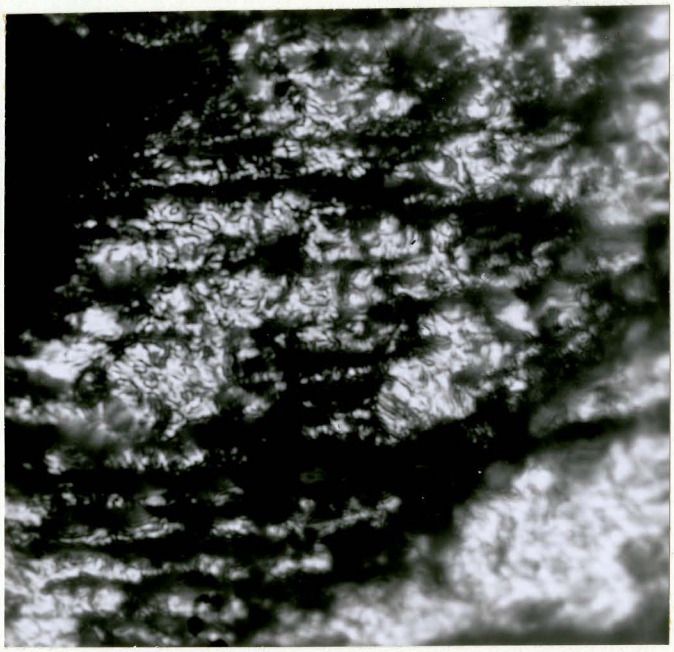

Figure 25. Optical micrograph of fatigue fracture surface. 400 x

Figure 26. Optical micrograph of fatigue fracture surface. 460 x

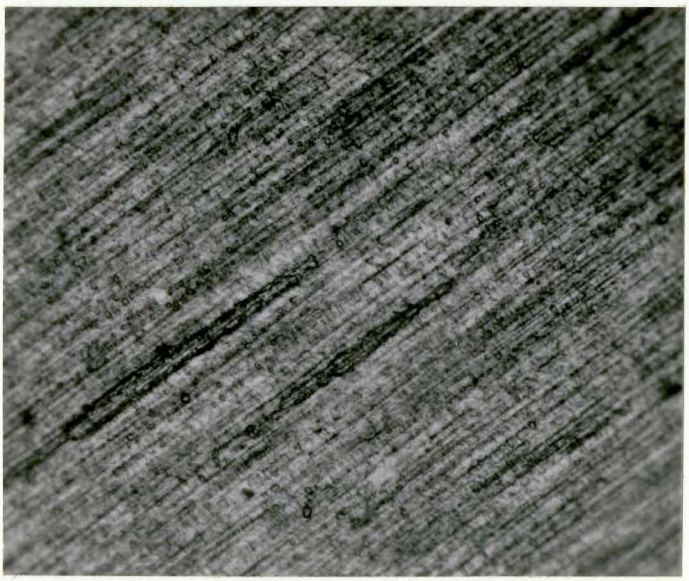

Figure 27. Polished and etched section of as received TD Nickel. Specimen axis from lower left to upper right on micrograph. 700 x

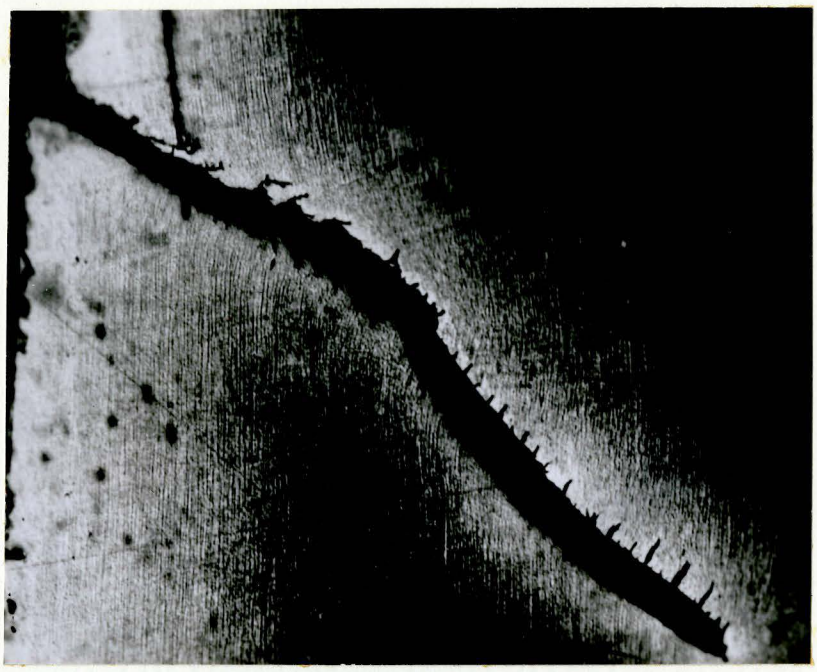

Figure 28. Section through fatigue crack. 148 x
Specimen axis vertical.

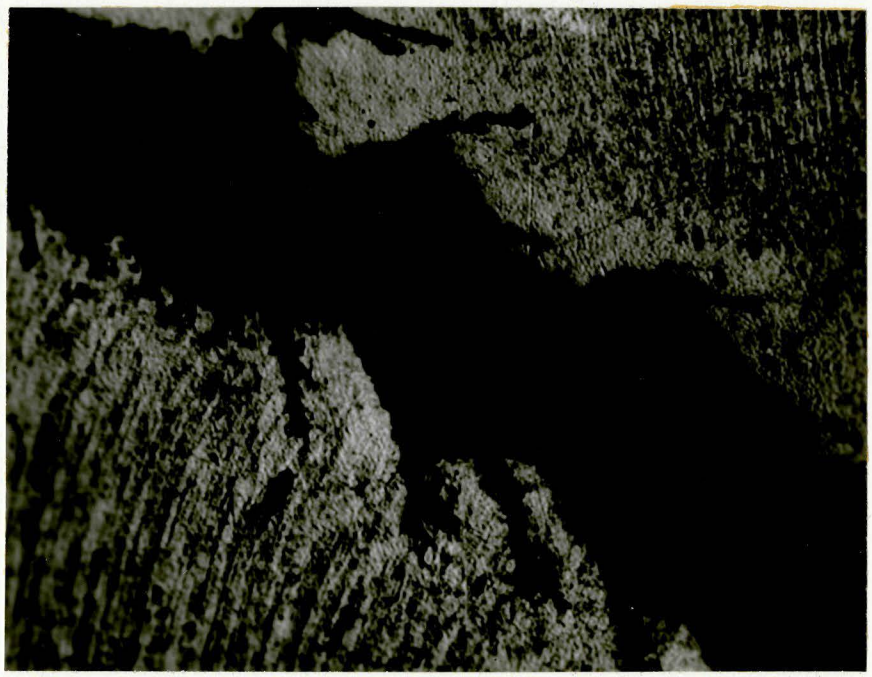

Figure 29. Section through fatigue crack. 880 x
Specimen axis vertical.

Figure 30. Section through fatigue crack. 350 x
Specimen axis vertical.

Figure 31. Section through fatigue crack. 460 x
Specimen axis vertical.

Figure 32. Tensile fracture surface. 16 x

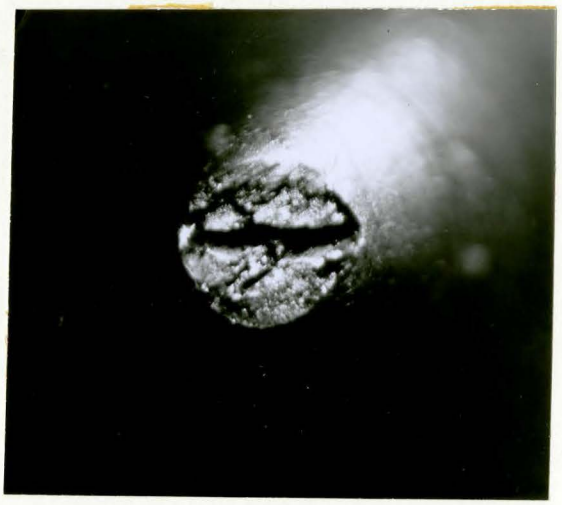

Figure 33. Tensile fracture surface. 22 x

Figure 34. Section parallel to specimen axis on tensile specimen with tensile neck on right. Specimen axis horizontal. 45 x

Figure 35. Section through root of axial crack. Specimen axis horizontal. 460 x

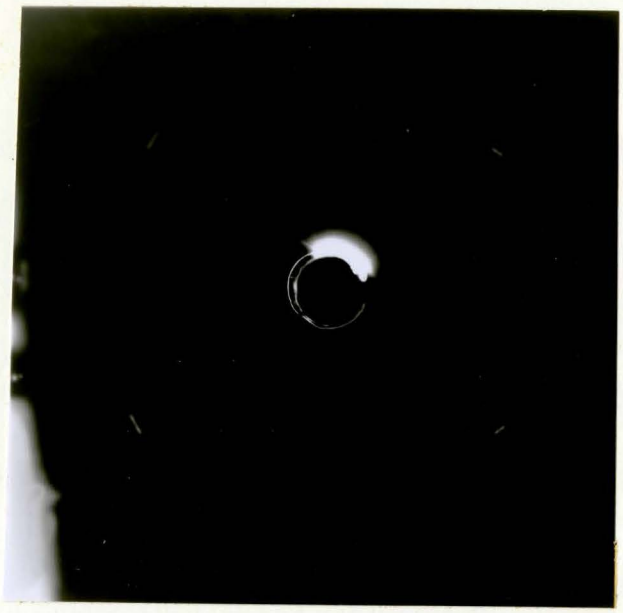

Figure 36. X-ray diffraction pattern showing fibre texture.

CHAPTER 6

DISCUSSION

This section is subdivided as follows. First the results of investigations into the structure of the as received material are summarized. Then the effects of this structure on the tensile and fatigue behaviors respectively are considered, showing how the tensile studies have a bearing on the interpretation of the fatigue results.

As received structure.

The important features of the structure before testing are the following. The grains are about 1 u in width and are elongated by a large factor in the direction of extrusion. Within each grain are a number of sub-grains which are also elongated. Thoria particles are dispersed throughout the structure and are stringered in the extrusion direction. Clusters of thoria particles are also present, these being spaced in the order of 0.5 u apart (on a planar section). The clusters are also strung out in the extrusion direction. Elongated intergranular voids occur with an average planar spacing of about 100 u. The material also has a very well developed $\langle 100 \rangle$ fibre texture.

Tensile fracture.

TD Nickel is quite ductile, necking to about 80% reduction in

area before failure. Tensile specimens with circular cross-sections develop cross-shaped axial fissures in their fracture surfaces. These unusual fissures can be explained by considering the triaxial state of stress in the necked region. In a plane perpendicular to the specimen axis, radial tensile stresses act as shown in Figure 37(a). These stresses, which are highest at the centre of the specimen, cause the formation of the cross-shaped cracks.

The numerous voids which exist in the necked region (Figure 35) provide a path for the propagation of these cracks. The concentration and shape of the voids can be explained by the distortion of the grain structure in the tensile neck. This distortion causes the axes of the grains to lie on cones pointing into the neck instead of lying parallel to each other. The elongated voids change their orientation in the same manner. On a planar section through these conically oriented voids, they appear shortened since they do not lie in the plane of the section unless the section bisects the cone (i.e., contains the specimen axis). Thus the voids appear to be elongated by a factor of only 2-3 in Figure 35. In addition, the concentration of voids in a planar section is increased by this distortion since the section cuts through many more grains than does an equivalent section through non-distorted material. Taking this factor into consideration, the concentration of voids in Figure 35 corresponds to that in as received TD Nickel.

This figure also shows that the path of the axial crack is determined by these elongated voids. In normal high purity materials where elongated voids are not present, this type of cracking cannot occur since even though the radial tensile stresses exist in the necked region, there is no such potential path along which an axial crack can propagate.

The specimen which necked unevenly did so because of a bending component in the applied stress. The distribution of radial stresses caused by the uneven necking is shown in Figure 37(b); however, this is modified by the bending. Since the bending effectively causes the necked area to move in the -x direction (Figure 37(b) it reduces the radial tensile stress in the +x direction. The resultant stress distribution is shown in Figure 37(c). This leads to the type of axial cracking shown in Figure 33.

Since the radial stresses in the neck fall to zero at the specimen surface, it is not surprising that the arms of the cross did not extend to this surface. The lack of cracking observed in the specimen which was sectioned after necking to 10% reduction in area indicates that considerable necking is required for the formation of the axial cross-shaped cracks.

Transmission electron microscopy of tensile specimens provided no evidence for the occurrence of particle-matrix detachment. It appears then that tensile stresses alone, or triaxial tensile stresses such as exist in the tensile neck are not capable of detaching particles from the matrix or causing cracks in the clusters of particles.

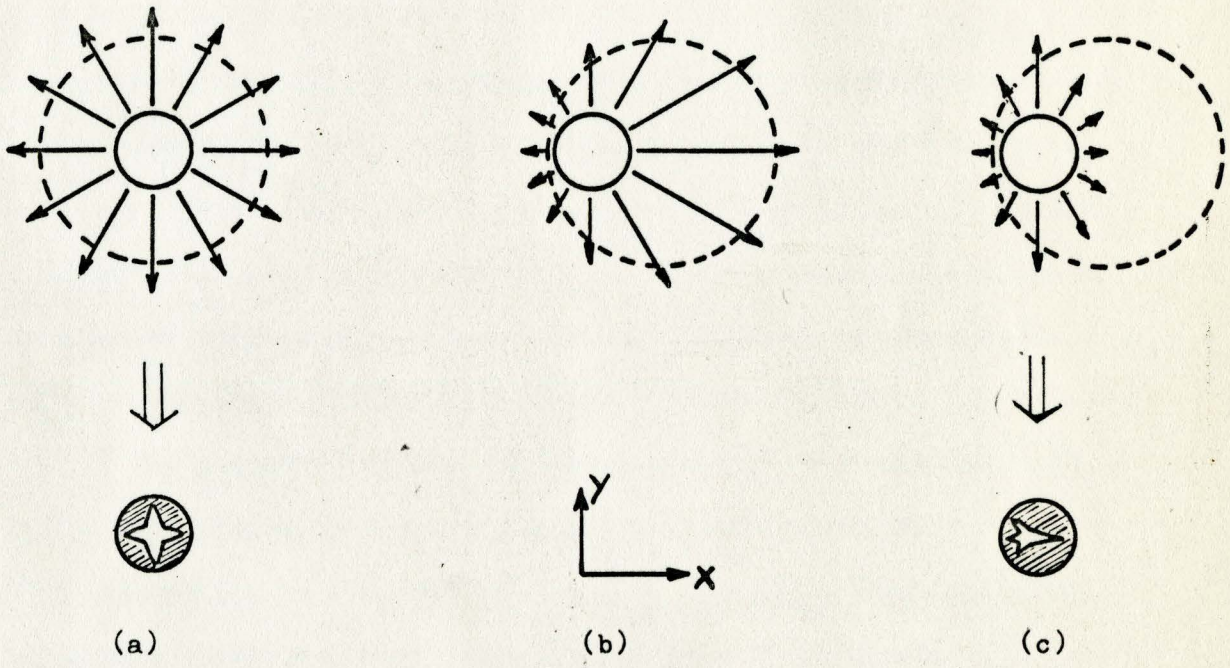

Figure 37. Radial stress distribution in tensile neck.

Broken line represents initial cross-section.

Solid line represents cross-section at fracture.

The tensile test on 0.025 in. thick sheet shows that shear failure can occur in this material under the correct conditions, namely a lack of necking (i.e. hydrostatic tension). This is plausible since the presence of the radial tensile stress at right angles to the applied tensile stress reduces the shear stresses which act in the plane of the two tensile stresses. This is shown on Figure 38. Shear stresses in the xz plane are much higher than those in the yz plane thus the material fractures as indicated. The fact that the material fractures in this manner indicates that it is more susceptible to shear failure than to normal stress failure since it would otherwise have failed by ductile rupture (cup and cone or double cup). However, despite the fact that TD Nickel is intrinsically weakest in shear, the presence of hydrostatic (triaxial tensile) stresses in the tensile neck prevent shear fracture from occurring whenever a specimen necks.

The presence of preferred orientation in this material reduces the tendency for shear failure (in the bulk specimens) since all four $\langle 111 \rangle$ planes lie at about 55° to the $\langle 100 \rangle$ direction (specimen axis), so that no single shear plane is formed. The sheet specimens were pulled in the Hounsfield tensometer, where axial constraints are less rigid. In this case some rotation can occur as the crack propagates, so as to confine the crack to the $\langle 111 \rangle$ planes on which it is growing. Thus once a shear crack is formed the inherent instability of the $\langle 100 \rangle$ orientation contributes to shear crack propagation.

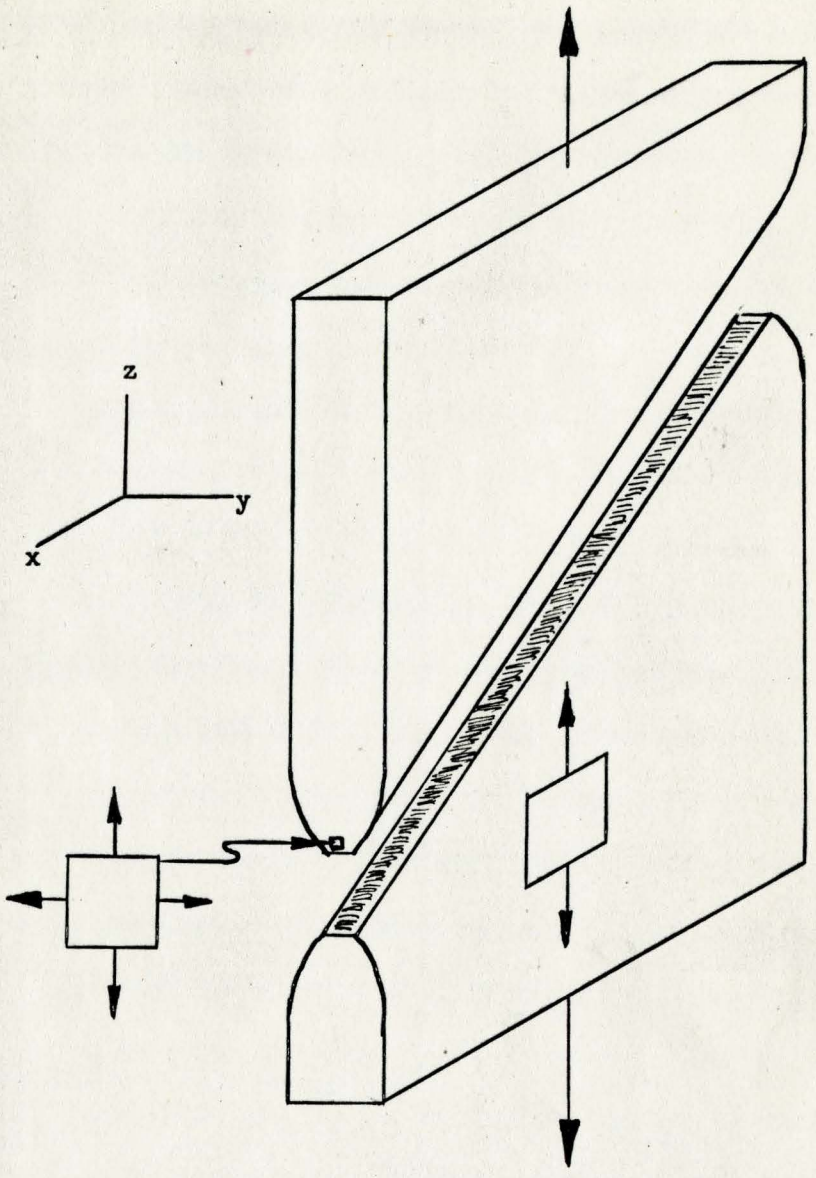

Figure 38. Tensile shear fracture of TD Nickel sheet.

The mechanism of fatigue failure in TD Nickel.

The initiation of fatigue fracture in TD Nickel occurs in a normal manner. The material fatigue softens, slip bands form in the direction of maximum shear stress, and cracks are initiated in these slip bands. There is no evidence that the thoria particles contribute directly to the initiation of fatigue cracks since if, particle-matrix detachment in the interior of the specimen was the cause of initiation, both the fatigue ratio and the appearance of the fatigue fracture surface would have been affected.

The onset of crack propagation, as indicated by a decrease in the peak tensile stress, occurred some 650 cycles before failure in specimens with fatigue lives of 8000 cycles. Thus approximately 8% of the life is spent in propagation, in good agreement with Laird and Smith (207) who found that for nickel and aluminum with fatigue lives of 10^4 cycles, 10% of life was spent in propagation.

The optical examination of fatigued specimens revealed striations on the fracture surfaces similar to those which form in normal stage II crack propagation. The number and spacing of these striations showed good agreement with the rate of crack propagation provided that each striation corresponds to one stress cycle. However, in TD Nickel the fracture surface lies at 45° to the stress axis rather than at 90°, indicating that the crack is not a conventional stage II type. Sections through fatigue cracks reveal sub-cracks with the same spacing as the striations, as well as grain distortion in the vicinity of the crack.

The fracture surface as revealed by electron fractographs corresponds to the regions between striations. The striations are so coarse that they usually fracture the carbon replica, although the "cliffs" shown in Figure 15 are likely due to these striations. The remainder of the features seen on electron fractographs, namely the irregular ridges (crevices in the specimen), craters (bumps on the specimen) and the linear texture are caused by crack growth within each cycle. In normal stage II fatigue crack propagation the regions between striations are featureless except for occasional sub-striations which are believed to be due to slip during the compressive half cycle (181). These disparities between the observed behavior and normal stage II behavior indicate that the latter is not the mode of fatigue failure in TD Nickel.

The fact that TD Nickel can fail in tension by shear (in the absence of necking) suggests that fatigue crack propagation may also be a shear process. Fatigue fracture by shear explains why the cracks propagate at 45° to the specimen axis and also explains the other observed features. Shear decohesion failure occurs in cold worked pure nickel fatigued at high stress (176,179,207). However in the pure nickel under these conditions no striations are observed on the fracture surface. It therefore appears that TD Nickel fractures by a mechanism intermediate between shear decohesion and conventional stage II fatigue crack growth. The proposed mechanism is as follows.

The crack initiates in a slip band (presumably at an intrusion). As it grows it has a tendency to turn normal to the stress axis so as to become a stage II fatigue crack. However, if it does this, it must

then penetrate through clusters of thoria particles. These clusters are not easily cracked by the hydrostatic tensile stress at the crack tip (as indicated by the lack of observed detachment in thin films from the necks of tensile specimens) but are more readily deformed by shear (as indicated by the tensile shear fracture of sheet). Thus if the crack turns to the normal stage II orientation it encounters more resistance from the thoria clusters than it does in growing by shear. This factor stabilizes propagation in the shear mode. The shear ahead of the growing fatigue crack thus penetrates the clusters and distorts the grain structure as shown in Figure 30. The presence of the $\langle 100 \rangle$ fibre texture enhances the ease of slip across grain boundaries. In addition, the inherent instability of this orientation also contributes to the ease of shear crack growth since a reorientation is necessary (once a crack is formed) to satisfy the demand of the fatigue machine for axiality as described in the discussion of tensile fracture.

The craters observed on the fracture surfaces are evidence for the contribution of thoria particle clusters to the fracture process. Thus spacing between craters is approximately the same as that between clusters and their sizes are also similar. The effect of penetration of a (shear) crack through a cluster is shown in Figure 39. It can be seen that this process leaves protrusions on the fracture surface. These, in turn, lead to craters in the fractograph since two-step replication creates an inversion of features.

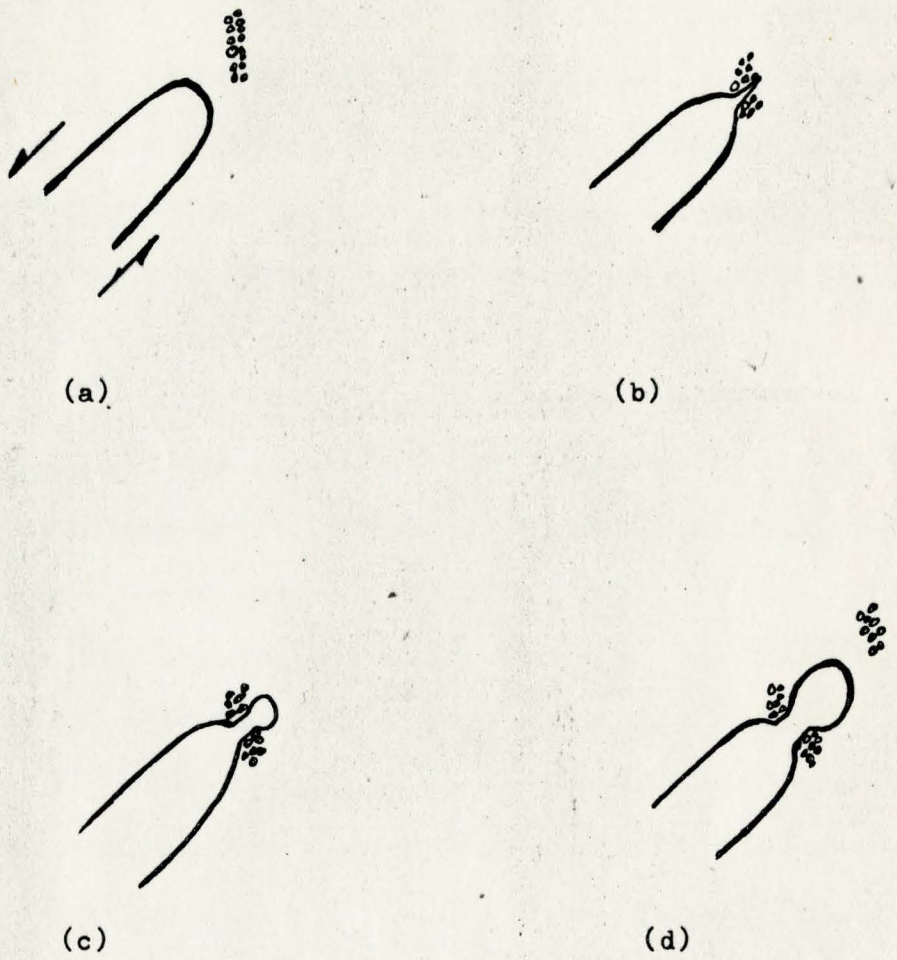

Figure 39. Penetration of a shear crack through a thoria particle cluster.

The irregularity which occurs during the compressive half cycle (Figure 7) provides further evidence that propagation is not a simple shear decohesion since if this were the case, this plastic flow would also be expected in the tensile half cycle. The irregularity can be explained by the following argument. As the crack grows by shear during the tensile half cycle, it is blunted by dislocation motion on planes at right angles to the plane of the crack. When the specimen is unloaded and re-loaded in compression, the stress reaches a value at which the crack is folded and resharpened. In these respects the process is similar to the Laird and Smith model for stage II propagation. However, in the case of TD Nickel this sharpening must involve shear so that the crack can grow through the thoria clusters. The extra increment of compressive strain is taken up by a shear displacement of the two faces of the crack so that a step appears on the specimen surface as shown in Figure 28.

As the crack grows, the uncracked area diminishes so that the sharpening strain occurs at lower values of compressive load (but the same compressive stress) so that the irregularity moves closer to zero load with each cycle. In addition, since the crack growth rate increases with cycling, the length of crack to be sharpened is also increased so that the amount of plastic strain due to the sharpening increases.

When the specimen is unloaded from compression and reloaded in tension, the crack grows to some extent by shear decohesion but it then becomes blunted by dislocation motion as described above. In addtion to this blunting action, slip on planes at 90° to the plane of the crack can cause the formation of sub-cracks. These shear type sub-cracks can be seen in Figure 28. It must be noted that sub-cracks can

be deformed by the subsequent folding of the crack front so that the observed orientations of the sub-cracks may not indicate the manner of their formation. Plastic deformation can also occur at the tip of the sub-cracks so that they grow as shown in Figure 29.

Sub-cracks can also be caused by the intergranular voids. Shear in the direction of crack growth can cause axial sub-cracks to develop (parallel to the elongated grain boundaries) whenever voids are encountered during the tensile half cycle. This effect can be seen on the upper face of the crack in Figure 29 and also in Figure 31.

In some cases a (shear type) sub-crack can become the most favourable path for continuation of crack propagation, so that the crack may turn by 90° as shown in Figure 30. This is particularly likely if the crack is growing away from the minimum cross-section of the specimen where the stresses are highest.

The sub-cracks, then, denote the successive positions of the crack front since they are formed during the tensile half cycle (blunting). They correspond to the striations seen on the fracture surface as in normal stage II propagation.

The fracture surfaces as revealed by electron fractographs correspond to the crack path between the striations. The curved ridges on the fractographs (crevices in the fracture surface) may be explained as follows. As the crack grows, it cuts through both high and low angle grain boundaries. When it cuts a high angle boundary its path will deviate slightly since the dislocation motion responsible for crack growth will then be taking place on planes with a slightly different orientation. If this orientation difference is large, the crack front is held up momentarily at the boundary. The boundary then tears (by

shear) and the crack grows into the new grain. This effect is expected to occur only at high angle boundaries with particularly unfavourable orientations, thus not all boundaries are revealed on the electron fractographs.

The direction of crack propagation is indicated by the direction in which the boundaries are sheared, and can therefore be determined by the tearing of the ridges on the micrograph. Figure 18 shows the result of this grain boundary tearing in a region in which many of the boundaries inhibit crack growth. In other regions many of the boundaries allow the crack to grow readily so that there is less boundary tearing. This may be related to the rate of crack growth since a slow-growing crack would be more easily delayed than would a rapidly growing crack.

The linear texture is due to slip accommodation at the face of the crack. Since the fracture plane is approximately a $\{111\}$ plane, the (shear) crack grows in the $\langle 110 \rangle$ direction. Slip lines on the crack surface occur at intersections of $\{111\}$ planes which are also $\langle 110 \rangle$ directions. In the electron fractographs which show the linear texture, this texture is always at either 60° or parallel to the direction of crack propagation (as indicated by the direction of grain boundary tearing) thus confirming that the texture is indeed caused by slip.

The striations in Figure 20 are believed to be the result of a temporary excursion into stage II cracking, likely near the origin of fracture. This could be caused by a region with an orientation particularly unfavourable for shear fracture.

The occasional surface areas which showed well defined parallel markings on electron fractographs (Figure 19) can be associated with the smooth regions on the optical fractographs (Figure 26) close to the final tensile fracture which followed fatigue. This final tensile fracture occurred by shear decohesion, thus these surfaces rubbed togehter as the specimen failed (the fatigued parts of the surfaces did not). This rubbing tends to smooth protruding areas of the surface, and score them by means of thoria clusters projecting from the sliding faces. This gives rise to the parallel scratch marks.

CHAPTER 7

CONCLUSIONS

1. No particle-matrix detachment occurs during either tensile or fully reversed axial fatigue stressing of TD Nickel.

2. Tensile fracture in bulk specimens is accompanied by cross-shaped axial cracks. These cracks form along paths provided by elongated voids, so as to relax the radial tensile stresses caused by necking. Tensile fracture in sheet specimens indicates that wherever possible this material fails by shear; however, necking inhibits shear fracture. The relative ease of failure in shear is attributed to the fact that crack propagation through clusters of thoria particles can occur more readily in shear than in tension.

3. Fatigue crack initiation occurs in the normal manner, by slip plane (shear) cracking. The propagation of fatigue cracks is controlled by the thoria particle clusters. Since cracks prefer to penetrate these clusters by shearing through them, fatigue crack growth is a shear controlled process which occurs at an angle of 45° to the stress (specimen) axis. Sub-cracks formed by stress reversal result in striations on the fatigue fracture surface. Thus fatigue crack growth in TD Nickel is a process intermediate between conventional stage II fatigue crack propagation and fatigue by shear decohesion.

CHAPTER 8

SUGGESTIONS FOR FUTURE WORK

1. In future work of this type it would be helpful to devise a method for determining the crack growth direction on electron fractographs.

2. A TD Nickel foil could be strained in an electron microscope tensile stage to observe the distortions and cracks forming in thoria clusters in the tensile neck.

3. A microbeam X-ray study of the fatigue fracture surface of TD Nickel would reveal whether subgrains were formed in the plastic zone at the crack tip. This has been observed by other workers in conventional materials. It would be interesting to see if the pre-existing substructure has an effect on this process.

4. X-ray line broadening experiments would reveal the extent to which relaxation of elastic strains contributes to the fatigue softening of TD Nickel. The fact that fatigue softening occurred with an increase in dislocation density is also significant and further work on thin film transmission electron microscopy of fatigue softening materials would help elucidate the mechanism of fatigue softening.

5. The role of grain boundaries in the fatigue and tensile fracture of TD Nickel could be studied by obtaining specimens which had been extruded and swaged to different diameters. Since these deformation operations determine the width and elongation of the grains, the difference in behavior of such specimens should help define the importance of the grain structure. Additional information could be obtained by rolling and recrystallizing TD Nickel, so as to drastically change the grain size. Since the elongated voids should be eliminated by the rolling operation, it would then be possible to assess the extent of cracking in thoria clusters.

APPENDIX A

Spark cutting is accomplished by the repeated discharge of a capacitor across a dielectric-filled gap between a tool and a workpiece. Each discharge causes a pulse of electrons to be accelerated across the gap where they bombard the surface of the workpiece. The result of this bombardment is localized melting of the workpiece (with ejection of resolidified metal particles into the dielectric) so that the tool gradually cuts through the specimen. However, in addition to this electron flux, there is a flux of positively charged ions (from dielectric breakdown) which bombard the tool. This causes the tool to be eroded until eventually it becomes useless. The standard tool used for cutting thin discs from a rod is a tungsten wire, typically 0.010 in. diameter. With use, the wire becomes thinner and finally breaks. When it is replaced, the new wire must be mounted so that it fits into the slot cut by the previous wire. Accurate alignment of the new wire is both necessary and difficult. Since as many as ten wires may be broken in cutting through a 0.375 in. diameter (nickel) rod, this alignment presents a major difficulty.

To eliminate this problem, a Servomet spark cutter was adapted to use a continuously moving wire as the cutting tool. This adaption was patterned after one designed by Dr. Z. S. Basinski of

the National Research Council, Ottawa. On a framework atop the spark cutter were mounted two 4 in. diameter reels and a drive system. One reel, the take-up reel, was continuously rotated by means of a "speedometer cable" drive (a Servomet accessory) acting through a pulley-belt system and a reduction gear, all of which were mounted on the framework. The other reel, the feed reel, rotated freely and held the unused wire. To guide the wire as it moved across the specimen, a copper fork was attached to the Servomet tool holder (see Figure A1). The wire was held in position by circumferentially grooved Teflon discs attached to each arm of the fork. Electrical contact was provided by a steel cylinder which was also mounted on the fork. Tension on the wire was maintained by friction in the bearings of the feed reel.

The variables which can be controlled when using this adaption include the wire tension, the speed of wire travel, the type and size of the wire, the spark gap (capacitance) range, the fine gap (voltage) control and the type of dielectric. These will be discussed in turn.

(i) The maximum wire tension is determined by the strength of the wire. At the other extreme, a certain amount of tension must be maintained to prevent the wire being forced too far away from the specimen by the energy of the spark. The tension could be varied by misaligning the feed reel bearings. The cutting rate was found to be relatively insensitve to tension.

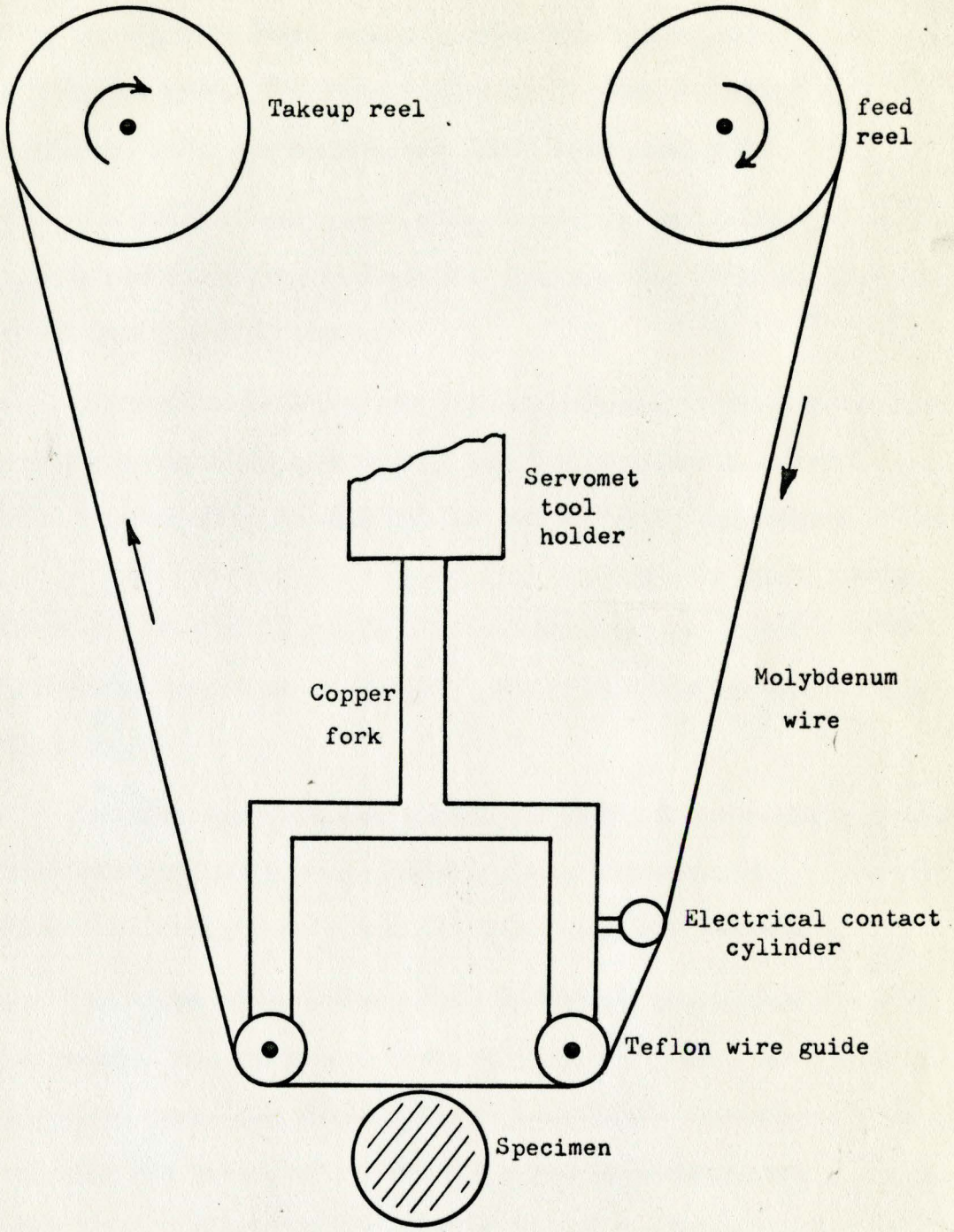

Figure A1. Spark cutting adaption.

(ii) The wire speed could be changed by using different sized pulleys in the belt drive system between the "speedometer cable" and the reduction gear. The slowest wire speed possible with this arrangement, 6 in. per minute, was found to be acceptable.

(iii) Two sizes of molybdenum wire, 0.0015 in. and 0.003 in. diameter were obtained from Sylvania Products, Towanda, Pa. Both sizes of wire were completely satisfactory.

(iv) The setting of the spark gap (capacitance) control determines the energy released by each spark. It is calibrated on a scale from 1 to 7, corresponding to high and low energy sparks respectively. It was found that when using the moving wire adaption the spark cutter could be operated on ranges 5,6 and 7 although range 5 could not be used with the fine wire. All spark cutting for this project was done on range 6.

(v) The fine spark control varies the width of the spark gap. This setting seriously affects the cutting rate. Unfortunately it was not possible to develop a technique for optimizing this adjustment.

(vi) Two types of dielectric fluid were used, automotive motor oil and kerosene. The latter was found to be superior when the moving wire adaption was used. The dielectric tends to become contaminated with carbon from the "cracking" of the dielectric hydrocarbon molecules in the spark gap. Filtration and circulation of the kerosene was attempted, however, it was found to be simpler to replace the kerosene when it became contaminated (every 100 operating hours).

Several additional problems arose during the operation of this apparatus. It was found that the wire must be kept free from kinks while it is being threaded through the fork, otherwise it breaks at a kink when the machine is started. Loose wire ends must be securely taped to the take-up spool to prevent them from arcing against the framework.

The heavier wire could be rewound onto the feed reel and re-used; however, the fine wire was discarded after use.

This apparatus, although unsophisticated, was used extensively with excellent results. With proper adjustment of the fine gap control it was possible to cut through a 0.375 in. diameter TD Nickel rod in less than 10 hours.

REFERENCES

1. Goetzel, C. G. and Bunshaw, R. F., Powder Metallurgy, Interscience, 1961, p. 253.

2. Irmann, R., Metallurgia 46, 125 (1952).

3. Lyle, J. P. Jr., Met. Prog. 62, 109 (1952) No. 6.

4. Goetzel, C. G., J. Met. 11, 189, 276 (1959).

5. Bloch, E. A., Met. Rev. 6, 193 (1961).

6. Guard, R. W., in Strengthening Mechanisms in Solids, ASM, 1962, p. 253.

7. Smith, G. C., Powder Met. 10, 102 (1963).

8. Kelly, A., in Electron Microscopy and the Strength of Crystals, Interscience, 1963, p. 947.

9. Kelly, A. and Nicholson, R. B., Prog. in Mat. Sci. 10 (1963) No. 3.

10. Kelly, A., Proc. Roy. Soc. A282, 63 (1964) No. 1388.

11. Grant, N. J., in The Strengthening of Metals, Reinhold, 1964, p. 163.

12. Cremens, W. S. and Grant, N. J., Proc. A.S.T.M. 58, 714 (1958).

13. Towner, R. J., Met. Prog. 73, 70 (1958) No. 5.

14. Meijering, J. L., Conf. on Strength of Solids, The Physical Society, 1948, p. 140.

15. Martin, J. W. and Smith, G. C., J. Inst. Met. 83, 417 (1955).

16. Preston, O. and Grant, N. J., Trans. AIME 221, 164 (1961).

17. Komatsu, N., Bonis, L. J. and Grant, N. J., Powder Metallurgy, Interscience, 1961, p. 343.

18. Ashby, M. F., in Electron Microscopy and the Strength of Crystals, Interscience, 1963, p. 891.

19. Worn, D. K. and Marton, S. F., Powder Metallurgy, Interscience, 1961, p. 343.

20. Tracey, V. A. and Worn, D. K., Powder Met. 10, 34 (1962).

21. Murphy, R. and Grant, N. J., Ibid, p. 1.

22. Chem. and Eng. News, 40, July 2, 1962, p. 40.

23. Anders, F. J., Alexander, G. B. and Wartel, W. S., Met. Prog. 82, 88 (1962) No. 6.

24. Mitchell, J. B., Mitra, S. K. and Dorn, J. E., Trans. ASM 56, 236 (1963).

25. Ashby, M. F., Z. Metallk. 55, 5 (1964).

26. Gensamer, M., Pearsall, E. B., Pellini, W. S. and Low, J. R. Jr., Trans. ASM 30, 983 (1942).

27. Roberts, C. S., Carruthers, R. C. and Averbach, B. L., Trans. ASM 44, 1150 (1952).

28. Lenel, F. V., Backensto, A. B. and Rose, M. V., Trans. AIME 209, 124 (1957).

29. Turkalo, A. M. and Low, J. R. Jr., Trans. AIME 212, 750 (1958).

30. Shaw, R. C., Shepard, L. A., Starr, C. D. and Dorn, J. E., Trans. ASM 45, 249 (1953).

31. Westbrook, J. H., Trans. ASM 45, 271 (1953).

32. Unckel, H., Metall. 5, 146 (1951).

33. Orowan, E., Symposium on Internal Stresses in Metals and Alloys, Institute of Metals, 1948, p. 451.

34. Nabarro, F. R. N., Ibid, p. 237.

35. Fullman, R. L., Trans. AIME 197, 447 (1953).

36. Gregory, E. and Grant, N. J., Trans. AIME 200, 247 (1954).

37. Dew-Hughes, D. and Robertson, W. D., Acta Met. 8, 147 (1960).

38. Lewis, M. H. and Martin, J. W., Acta Met. 11, 1207 (1963).

39. Tyson, W. R., Acta Met. 11, 61 (1963).

40. Ashby, M. F. and Smith, G. C., Phil. Mag. 5, 298 (1960).

41. Nicholson, R. B., Thomas, G. and Nutting, J., Acta Met. 8, 172 (1960).

42. Bonar, L. G. and Kelly, A., Proc. Fifth International Conference for Electron Microscopy, Academic, 1962, p. K11.

43. Koda, S., Morozumi, S. and Kikuchi, M., J. Inst. Met. 93, 449 (1965).

44. Ansell, G. S. and Lenel, F. V., Acta Met. 8, 612 (1960).

45. Lenel, F. V. and Ansell, G. S., Powder Metallurgy, Interscience, 1961, p. 267.

46. Ansell, G. S., Acta Met. 9, 518 (1961).

47. Lenel, F. V., Ansell, G. S. and Bosch, R. A., Trans. AIME 221, 892 (1961).

48. Ansell, G. S., in High Temperature Materials Technology, Butterworths, 1964, p. 325.

49. Goodrich, R. S. and Ansell, G. S., Acta Met. 12, 1097 (1964).

50. Lenel, F. V., Ansell, G. S. and Nelson, E. C., Trans. AIME 209, 117 (1957).

51. Meiklejohn, W. H. and Skoda, R. E., Acta Met. 8, 773 (1960).

52. Abel, A. and Ham, R. K., to be published in Acta Met.

53. Keeler, J. H., Trans. ASM 48, 825 (1956).

54. Keeler, J. H., Trans. AIME 206, 486 (1956).

55. Hibbard, W. R. and Hart, E. W., Trans. AIME 203, 200 (1955).

56. Hirsch, P. B., J. Inst. Met. 86, 13 (1958).

57. Swann, P. R., in Electron Microscopy and the Strength of Crystals, Interscience, 1963, p. 131.

58. von Heimendahl, M. and Thomas, G., Trans. AIME 230, 1520 (1964).

59. Greetham, G. and Honeycombe, R. W. K., J. Inst. Met. 89, 13 (1960).

60. Byrne, J. G., Fine, M. E. and Kelly, A., Phil. Mag. 6, 1119 (1961).

61. Mott, N. F. and Nabarro, F. R. N., Proc. Phys. Soc. 52, 86 (1940).

62. Goodrich, R. S. and Ansell, G. S., Trans. AIME 230, 1372 (1964).

63. Fleischer, R. L., in Electron Microscopy and the Strength of Crystals, Interscience, 1963, p. 973.

64. Hart, E. W., in The Relation of Properties to Microstructure, ASM, 1953, p. 95.

65. Gregory, E. and Smith, G. C., J. Inst. Met. 85, 81 (1956).

66. Fisher, J. C., Hart, E. W. and Pry, R. H., Acta Met. 1, 336 (1953).

67. Gatti, A. and Fullman, R. L., Trans. AIME 215, 762 (1959).

68. Bullen, F. P., Ryan, N. E. and Rogers, C. B., Phil. Mag. 10, 903 (1964).

69. Carlsen, K. M. and Honeycombe, R. W. K., J. Inst. Met. 83, 449 (1955).

70. Price, R. J. and Kelly, A., Acta Met. 10, 980 (1962).

71. Jones, D. A. and Mitchell, J. W., Phil. Mag. 3, 1 (1958).

72. Huggins, R. A., Acta Met. 7, 357 (1959).

73. Ashby, M. F. and Smith, G. C., J. Inst. Met. 91, 182 (1963).

74. Brimhall, J. L. and Huggins, R. A., Trans. AIME 233, 1076 (1965).

75. Friedel, J., in Electron Microscopy and the Strength of Crystals, Interscience, 1963, p. 605.

76. Hirsch, P. B., in Internal Stresses and Fatigue in Metals, Elsevier, 1959, p. 139.

77. Klein, M. J. and Huggins, R. A., Acta Met. 10, 55 (1962).

78. Barnby, J. T. and Smith, E., Acta Met. 12, 1353 (1964).

79. King, G. W. and Sell, H. G., Trans. AIME 233, 1104 (1965).

80. Grant, N. J. and Preston, O., Trans. AIME 209, 349 (1957).

81. Grierson, R. and Bonis, L. J., Ilikon Corp. Paper NASw-726, May 1965.

82. Averbach, B. L., Bever, M. B., Comerford, M. F. and Leach, J. S. L., Acta Met. 4, 477 (1956).

83. Adachi, M. and Grant, N. J., Trans. AIME 218, 881 (1960).

84. Imai, Y. and Hirotani, H., Powder Metallurgy, Interscience, 1961, p. 359.

85. Wilson, D. V. and Konnan, Y. A., Acta Met. 12, 617 (1964).

86. White, J. E. and Carnahan, R. D., Trans. AIME 230, 1298 (1964).

87. Clark, C. A. and Mee, P. B., Z. Metallk. 53, 756 (1962).

88. Inman, M. C., Zwilsky, K. M. and Boone, D. H., Trans. ASM 57, 701 (1964).

89. Thomas, G. and Nutting, J., J. Inst. Met. 86, 7 (1958).

90. Dew-Hughes, D. and Robertson, W. D., Acta Met. 8, 156 (1960).

91. Price, R. J. and Kelly, A., Acta Met. 11, 915 (1963).

92. Ansell, G. S. and Kim, H. S., Powder Met. 10 (1962).

93. Lewis, M. H., Seebohm, R. H. and Martin, J. W., Ibid.

94. Gurland, J., Trans. AIME 221, 406 (1961).

95. Johnston, T. L, Stokes, R. J. and Li, C. H., Ibid, p. 792.

96. Edelson, B. I. and Baldwin, W. M. Jr., Trans. ASM 55, 230 (1962).

97. Gurland, J. and Plateau, J., Trans. ASM 56, 442 (1963).

98. Gilbert, A., Ratliff, J. L. and Warke, W. R., Trans. ASM 58, 142 (1965).

99. Stuart, R. E. and Starr, C. D., Mat. in Des. Eng., August 1963.

100. Wilcox, B. A. and Clauer, A. H., Trans. AIME 233, 253 (1965).

101. Doble, G. S. and Quigg, R. J., Trans. AIME 233, 410 (1965).

102. Sims, C. T., Trans. AIME 227, 1455 (1963).

103. Forsyth, P. J. E., in Fatigue in Aircraft Structures, Academic Press, 1956, p. 20.

104. Thompson, N. and Wadsworth, N. J., Adv. in Phys. 7, 72 (1958).

105. Parker, E. R. and Fegredo, D. M., in Internal Stresses and Fatigue in Metals, Elsevier, 1959, p. 263.

106. Thompson, N., Z. Metallk. 53, 71 (1962).

107. Low, J. R. Jr., Prog. Mat. Sci. 12 (1963) No. 1.

108. Kennedy, A. J., Brit. J. Appl. Phys. 15, 229 (1964).

109. Kemsley, D. S. and Patterson, M. S., Acta Met. 8, 453 (1960).

110. Wadsworth, N. J., Acta Met. 11, 663 (1963).

111. Thompson, N., Wadsworth, N. J. and Louat, N., Phil. Mag. 1, 113 (1956).

112. Wood, W. A. and Segall, R. L., Proc. Roy. Soc. A242, 180 (1957).

113. Ebner, M. L. and Backofen, W. A., Trans. AIME 215, 510 (1959).

114. Alden, T. H. and Backofen, W. A., Acta Met. 9, 352 (1961).

115. Segall, R. L., in Electron Microscopy and the Strength of Crystals, Interscience, 1963, p. 515.

116. Backofen, W. A., in Fracture, Wiley, 1959, p. 435.

117. Broom, T. and Ham, R. K., Proc. Roy. Soc. A242, 166 (1957).

118. Thompson, N., in Fatigue of Aircraft Structures, Academic Press, 1956, p. 43.

119. Smith, G. C., Proc. Roy. Soc. A242, 189 (1957).

120. Mott, N. F., in Dislocations and Mechanical Properties of Crystals, Wiley, 1957, p. 458.

121. Polakowski, N. H. and Palchoudhuri, A., Proc. A.S.T.M. 54, 701 (1954).

122. Kemsley, D. S., J. Inst. Met. 87, 10 (1958).

123. Wood, W. A. and Segall, R. L., J. Inst. Met. 86, 225 (1958).

124. Dugdale, D. S., J. Mech. Phys. Sol. 7, 135 (1959).

125. Benham, P. P., J. Inst. Met. 89, 328 (1961).

126. Hein, E. and Dodd, R. A., Trans. AIME 221, 1095 (1961).

127. Ham, R. K. and Broom, T., Phil. Mag. 7, 95 (1962).

128. Benham, P. P., J. Inst. Met. 91, 404 (1963).

129. Raymond, M. H. and Coffin, L. F., Acta Met. 11, 817 (1963).

130. Feltner, C. E. and Laird, C., paper presented at the Fall Meeting of AIME, October 1965, Detroit.

131. Snowden, K. U., Acta Met. 11, 675 (1963).

132. Segall, R. L. and Partridge, P. G., Phil. Mag. 4, 912 (1959).

133. Segall, R. L., Partridge, P. G. and Hirsch, P. B., Phil. Mag. 6, 1493 (1961).

134. Pelloux, R. M. N., Boeing Co. Report D1-82-0304, October 1963.

135. Feltner, C. E., Phil. Mag. 12, 1229 (1965).

136. Wilson, R. N. and Forsyth, P. J. E., J. Inst. Met. 87, 336 (1959).

137. Thomas, K., in Proc. Fifth International Conference for Electron Microscopy, Academic Press, 1962, p. J-6.

138. Grosskreutz, J. C. and Waldow, P., Acta Met. 11, 717 (1963).

139. Holden, J., Acta Met. 11, 691 (1963).

140. Grosskreutz, J. C., J. Appl. Phys. 34, 372 (1963).

141. Feltner, C. E., Acta Met. 11, 817 (1963).

142. Pratt, J. E., paper presented at the Fall Meeting of AIME, October 1965, Detroit.

143. Avery, D. H. and Backofen, W. A., in Fracture of Solids, Interscience, 1963, p. 339.

144. Hirsch, P. B., Partridge, P. G. and Segall, R. L., Phil. Mag. 4, 721 (1959).

145. Feltham, P., Phil. Mag. 6, 1479 (1961).

146. Avery, D. H. and Backofen, W. A., Acta Met. 11, 653 (1963).

147. Forsyth, P. J. E., J. Inst. Met. 80, 181 (1951).

148. Laufer, E. and Roberts, N., Phil. Mag. 10, 883 (1964).

149. McGrath, J. T. and Waldron, G. W. J., Phil. Mag. 9, 249 (1964).

150. Forsyth, P. J. E. and Stubbington, C. A., J. Inst. Met. 83, 395 (1954).

151. Kemsley, D. S., J. Inst. Met. 85, 420 (1956).

152. Wood, W. A., in Fatigue in Aircraft Structures, Academic Press, 1956, p. 1.

153. Grosskreutz, J. C., J. Appl. Phys. 33, 1787 (1962).

154. Stubbington, C. A. and Forsyth, P. J. E., J. Inst. Met. 86, 90 (1957).

155. Wadsworth, N. J. and Hutchings, J., Phil. Mag. 3, 1154 (1958).

156. Thompson, N., in Fracture, Wiley, 1959, p. 354.

157. McEvily, A. J. Jr. and Boettner, R. C., Acta Met. 11, 725 (1963).

158. McEvily, A. J. Jr. and Boettner, R. C., in Fracture of Solids, Interscience, 1963, p. 383.

159. Forsyth, P. J. E., Nature 171, 172 (1953).

160. Hull, D., J. Inst. Met. 84, 527 (1956).

161. Forsyth, P. J. E., Proc. Roy. Soc. A242, 198 (1957).

162. Hull, D., J. Inst. Met. 86, 425 (1957).

163. Forsyth, P. J. E., Acta Met. 11, 703 (1963).

164. Wood, W. A., Cousland, S. McK. and Sargant, K. R., Acta Met. 11, 643 (1963).

165. Wood, W. A., in Fracture, Wiley, 1959, p. 354.

166. Forsyth, P. J. E. and Stubbington, C. A., J. Inst. Met. 85, 339 (1957).

167. Cottrell, A. H. and Hull, D., Proc. Roy. Soc. A242, 211 (1957).

168. Mott, N. F., Acta Met. 6, 195 (1958).

169. McEvily, A. J. Jr. and Machlin, E. S., in Fracture, Wiley, 1959, p. 450.

170. Watt, D. F., to be published.

171. Chin, G. Y. and Backofen, W. A., J. Inst. Met. 90, 13 (1961).

172. Forsyth, P. J. E., J. Inst. Met. 82, 449 (1954).

173. Forsyth, P. J. E., Proceedings of the Cranfield Symposium, 1961, p. 76.

174. Forsyth, P. J. E. and Ryder, D. A., Metallurgia 63, 117 (1961).

175. Plateau, J., Crussard, C., Faguet, J., Henry, G., Weisz, M., Sertour, G. and Esquerre, R., Rev. Mét. 55, 679 (1958).

176. Crussard, C., Plateau, J., Tanhankar, R., Henry, G. and Lajeunesse, D., in Fracture, Wiley, 1959, p. 524.'

177. Pelloux, R. M. N., ASM Preprint TR-P-19-3-64, October 1964.

178. Jacoby, G., Exp. Mech. 5, 65 (1965).

179. Laird, C. and Smith, G. C., Phil. Mag. 7, 847 (1962).

180. Williams, M. L., J. Appl. Mech. 24, 109 (1957).

181. Boettner, R. C., Laird, C. and McEvily, A. J. Jr., Trans. AIME 233, 379 (1965).

182. Holden, J., Phil. Mag. 6, 547 (1961).

183. Frost, N. E., Holden, J. and Phillips, C. E., Proceedings of the Cranfield Symposium, 1961, p. 166.

184. Wood, W. A., Riemann, W. H. and Sargant, K. R., Trans. AIME 230, 511 (1964).

185. Holden, J., in Fatigue Resistance of Materials and Metal Structural Parts, Macmillan, 1964, p. 113.

186. Forsyth, P. J. E. and Stubbington, C. A., J. Inst. Met. 83, 173 (1955).

187. Elwood, E. C. and Duckett, D., Nature 173, 497 (1954).

188. Honeycombe, R. W. K., Proc. Roy. Soc. A242, 213 (1957).

189. McGrath, J. T., Can. Met. Quart. 2, 347 (1963).

190. Abel, A., M.Sc. Thesis, McMaster University, 1965.

191. Liu, S. I. and Sachs, G., Trans. AIME 180, 193 (1949).

192. Wilson, D. V., Acta Met. 13, 807 (1965).

193. Clark, J. B. and McEvily, A. J. Jr., Acta Met. 12, 1359 (1964).

194. Hempel, M. R., in Fracture, Wiley, 1959, p. 376.

195. Classman, L. H. and McEvily, A. J. Jr., NASA TN-D-928 (Apr. 1962).

196. Lyst, J. O., Mat. Res. and Stds, 2, 751 (1962).

197. Pelloux, R. M. N., Trans. ASM 57, 511 (1964).

198. Stubbington, C. A., Acta Met. 12, 931 (1964).

199. Broom, T., Molineux, J. H. and Whittaker, V. N., J. Inst. Met. 84, 357 (1956).

200. Ransom, J. T., Trans. ASM 46, 1254 (1954).

201. Dieter, G. E., Mehl, R. F. and Horne, G. T., Trans. ASM 47, 423 (1955).

202. Cummings, H. N., Stulen, F. B. and Schultz, W. C., Trans. ASM 49, 482 (1957).

203. Chodorowski, J. and Boch, A., in Fatigue Resistance of Materials and Metal Structural Parts, Macmillan, 1964, p. 161.

204. Wells, C. H. and Sullivan, C. P., Trans. ASM 57, 841 (1964).

205. Martin, J. W. and Smith, G. C., J. Inst. Met. 83, 153 (1955).

206. Doyle, W. M., J. Inst. Met. 84, 526 (1956).

207. Laird, C. and Smith, G. C., Phil. Mag. 8, 1945 (1963).